

Alma Mater Studiorum Università di Bologna
Archivio istituzionale della ricerca

CDKL5 protein substitution therapy rescues neurological phenotypes of a mouse model of CDKL5 disorder

This is the final peer-reviewed author's accepted manuscript (postprint) of the following publication:

Published Version:

Trazzi, S., De Franceschi, M., Fuchs, C., Bastianini, S., Viggiano, R., Lupori, L., et al. (2018). CDKL5 protein substitution therapy rescues neurological phenotypes of a mouse model of CDKL5 disorder. HUMAN MOLECULAR GENETICS, 27(9), 1572-1592 [10.1093/hmg/ddy064].

Availability:

This version is available at: <https://hdl.handle.net/11585/655847> since: 2019-01-22

Published:

DOI: <http://doi.org/10.1093/hmg/ddy064>

Terms of use:

Some rights reserved. The terms and conditions for the reuse of this version of the manuscript are specified in the publishing policy. For all terms of use and more information see the publisher's website.

This item was downloaded from IRIS Università di Bologna (<https://cris.unibo.it/>).
When citing, please refer to the published version.

(Article begins on next page)

This is the final peer-reviewed accepted manuscript of:

Trazzi S, De Franceschi M, Fuchs C, Bastianini S, Viggiano R, Lupori L, Mazziotti R, Medici G, Lo Martire V, Ren E, Rimondini R, Zoccoli G, Bartesaghi R, Pizzorusso T, Ciani E.

CDKL5 protein substitution therapy rescues neurological phenotypes of a mouse model of CDKL5 disorder.

Hum Mol Genet. 2018 May 1;27(9):1572-1592

The final published version is available online at: <https://doi.org/10.1093/hmg/ddy064>

Rights / License:

The terms and conditions for the reuse of this version of the manuscript are specified in the publishing policy. For all terms of use and more information see the publisher's website.

This item was downloaded from IRIS Università di Bologna (<https://cris.unibo.it/>)

When citing, please refer to the published version.

CDKL5 PROTEIN SUBSTITUTION THERAPY RESCUES NEUROLOGICAL PHENOTYPES OF A MOUSE MODEL OF CDKL5 DISORDER

Stefania Trazzi^{1*}, Marianna De Franceschi^{1*}, Claudia Fuchs^{1**}, Stefano Bastianini^{1**}, Rocchina Viggiano¹,
Leonardo Lupori⁵, Raffaele Mazziotti³, Giorgio Medici¹, Viviana Lo Martire¹, Elisa Ren¹, Roberto
Rimondini³, Giovanna Zoccoli¹, Renata Bartesaghi¹, Tommaso Pizzorusso^{2,3,5}, Elisabetta Ciani¹

¹Department of Biomedical and Neuromotor Sciences, University of Bologna, Italy; ²Institute of Neuroscience, CNR Pisa Italy; ³NEUROFARBA Department, University of Florence, Italy, ⁴Department of Medical and Clinical Sciences, University of Bologna, Italy. ⁵BIO@SNS lab, Scuola Normale Superiore di Pisa, Italy

* Authors labeled with an asterisk contributed equally to the work.

** Authors labeled with two asterisks contributed equally to the work.

CORRESPONDING AUTHOR: Prof. Elisabetta Ciani,

Department of Biomedical and Neuromotor Sciences,

Piazza di Porta San Donato 2, 40126 Bologna, Italy.

Tel +39 051 2091773

Fax +39 051 2091737

E-mail elisabetta.ciani@unibo.it

ABSTRACT

Cyclin-dependent kinase like-5 (CDKL5) disorder is a rare neurodevelopmental disease caused by mutations in the *CDKL5* gene. The consequent misexpression of the CDKL5 protein in the nervous system leads to a severe phenotype characterized by intellectual disability, motor impairment, visual deficits, and early-onset epilepsy. No therapy is available for CDKL5 disorder. It has been reported that a protein transduction domain (TAT) is able to deliver macromolecules into cells and even into the brain when fused to a given protein. We demonstrate that TAT-CDKL5 fusion protein is efficiently internalized by target cells and retains CDKL5 activity. Intracerebroventricular infusion of TAT-CDKL5 restored hippocampal development, hippocampus-dependent memory and breathing pattern in *Cdkl5*-null mice. Notably, systemically-administered TAT-CDKL5 protein passed the blood-brain-barrier, reached the CNS, and rescued various neuroanatomical and behavioral defects, including breathing pattern and visual responses. Our results suggest that CDKL5 protein therapy may be an effective clinical tool for the treatment of CDKL5 disorder.

INTRODUCTION

CDKL5 (cyclin-dependent kinase-like 5) disorder is a severe X-linked neurodevelopmental disease caused by mutations in the *CDKL5* gene, which lead to a lack of CDKL5 protein expression or function. The CDKL5-related encephalopathy affects mostly girls and, due to the numerous clinical features that overlap with the better-characterized Rett syndrome (RTT), it was initially termed as an “early seizure variant” or “Hanefeld variant” of RTT. Similarities between RTT and CDKL5 encephalopathy are related to the severe neurodevelopmental impairment, intellectual disability, motor impairment, and in some cases respiratory dysregulation. However, a systematic analysis of clinical symptoms across patients has led to the conclusion that CDKL5 disorder is a distinct clinical entity characterized by early-onset epileptic seizures (in the first few months of life), hypotonia, abnormal eye tracking, and severe visual impairment (1-4).

CDKL5 is highly expressed in the brain, mainly in neurons with both a nuclear and dendritic localization (5-8). In the early postnatal period, CDKL5 brain expression exhibits a peak (6, 8), suggesting its potential importance in brain maturation. Animal models of CDKL5 disorder, *Cdkl5* knockout (KO) mice (9-11), have recently been created to clarify the role of CDKL5 in brain development and in the etiology of CDKL5 disorder. *Cdkl5* KO mice recapitulate different features of CDKL5 disorder, exhibiting severe impairment in hippocampus-dependent learning and memory, visual and respiratory deficits, and motor stereotypies (9, 10, 12, 13). These defects are associated with neuroanatomical alterations, such as reduced dendritic arborization of hippocampal and cortical neurons, reduced dendritic spine density, and altered connectivity (10, 12-16).

The failure of proteins to penetrate the cell membrane prevents their use as a therapeutic tool in a variety of monogenic disorders caused by the lack of function of a single protein. Recently, protein transduction domains (PTDs) have been shown to promote the delivery of proteins into living cells and through the blood brain barrier. PTDs are small peptides that are able to ferry much larger molecules into cells independently, by classical endocytosis (17). The HIV-1 Transactivator of Transcription (TAT) protein is the best characterized viral PTD containing protein. Earlier experiments with the TAT-PTD protein domain demonstrated successful transduction of fusion proteins up to 120 kDa into murine cells (18-20). Schwarze et al. (19) reported that a recombinant TAT- β -galactosidase protein, injected intraperitoneally into

mice, was distributed to all tissues, including the brain, and retained its biological activity. Importantly, the TAT-PTD has not been reported to have any toxic effects or immunogenicity problems so far (17).

Although pharmacological treatments are used to control seizures, no cure or effective treatments are currently available to ameliorate cognitive and behavioral symptoms for CDKL5 disorder. The aim of this study was to develop a protein substitution therapy for CDKL5 disorder in order to compensate for the lack of function of the CDKL5 protein. We produced a TAT-CDKL5 protein that was efficiently transduced into cells, and subsequently evaluated whether central and peripheral administration of this fusion protein improves brain development and behavior in a mouse model of CDKL5 disorder.

RESULTS

Target cells are efficiently transduced by TAT κ -CDKL5 fusion protein

Alternative splice isoforms for the human *CDKL5* gene have been described (21, 22). The original CDKL5 transcript generates a protein of 1030 amino acids (CDKL5_s (22), 115 kDa). While CDKL5_s is the first characterized CDKL5 isoform, a recently identified transcript, characterized by an altered C-terminal region, is likely to be relevant for CDKL5 brain functions (CDKL5_l(22), 107 kDa) (23). No knowledge as to a different activity of the CDKL5 isoforms is currently available. To identify which CDKL5 isoform was more suitable for a protein therapy, we produced both TAT κ -CDKL5_l and TAT κ -CDKL5_s fusion proteins and compared their production and activity. Since full length CDKL5 protein cannot be produced in bacteria (24), we induced the expression of the TAT κ -CDKL5 recombinant protein in mammalian cells. In order to enhance protein recovery, we took advantage of a synthetic TAT κ -PTD in which mutation of the furin recognition sequences, but retention of protein transduction activity, allows secretion of recombinant proteins (25). Due to the absence of a suitable anti-CDKL5 antibody that works on brain tissue, the TAT κ -CDKL5 fusion proteins were tagged with a GFP protein to monitor their expression levels.

Western blot analysis detected high levels of TAT κ -GFP-CDKL5_l (Fig. 1A) and TAT κ -GFP-CDKL5_s (Supplementary Material Fig. S2A) proteins in the culture medium 48 h after transfection of

HEK293T cells, indicating that both TATκ-GFP-CDKL5 proteins were efficiently secreted from these cells. However, the recovery of TATκ-GFP-CDKL5₁ fusion protein from the culture medium was higher than that of TATκ-GFP-CDKL5₅ (Supplementary Material Fig. S2A), suggesting a more efficient secretion of the shorter CDKL5 isoform (CDKL5₁).

To investigate whether target cells were transduced with the secreted TATκ-GFP-CDKL5 proteins, hippocampal neurons were incubated with the purified TATκ-GFP-CDKL5₁ protein. After 1h of incubation, cells were lysed and total protein extracts were immunoblotted for TATκ-GFP-CDKL5₁ protein quantification. As shown in Figs. 1B-C, TATκ-GFP-CDKL5₁ is efficiently internalized by target cells. The internalization in target cells was confirmed by confocal microscopy (Fig. 1D). Fig. 1D shows serial confocal images of TATκ-GFP-CDKL5₁ transduced hippocampal neurons, demonstrating that TATκ-GFP-CDKL5₁ protein is internalized by target cells and localized mainly in the cytoplasm, consistent with CDKL5 cellular distribution (7). Similar results for transduction efficiency were obtained with the TATκ-GFP-CDKL5₅ fusion protein (Supplementary Material Fig. S2B).

The efficacy of protein therapeutics are limited by pharmaceutical issues among which the most important is the protein half-life. We found that, when transduced into cells, the TATκ-GFP-CDKL5₁ half-life was about 12 h (Supplementary Material Fig. S2D), suggesting an intracellular stability of the fusion protein that is appropriate for *in vivo* treatments.

TATκ-CDKL5 fusion protein retains wild type activity

Since CDKL5 is known to inhibit proliferation of neuroblastoma cells (26), we evaluated TATκ-GFP-CDKL5 fusion protein activity by treating SH-SY5Y neuroblastoma cells with purified TATκ-GFP-CDKL5₁, TATκ-GFP-CDKL5₅ or TATκ-GFP protein as controls (Fig. 2A-C, Supplementary Material Fig. S2C). The increase of CDKL5 protein levels within neuroblastoma cells, through TATκ-GFP-CDKL5₁ protein treatment (Fig. 2C), caused a strong inhibition of cell proliferation (evaluated as a mitotic index, Fig. 2A,B) compared to control treatment (TATκ-GFP). We found that TATκ-GFP-CDKL5₅ isoform has the same antiproliferative activity as TATκ-GFP-CDKL5₁ isoform on neuroblastoma cells (Fig. 2A,B; Supplementary Material Fig. S2C), suggesting a similar physiological activity. Considering that the addition of GFP may alter the activity of CDKL5, we compared the activity of the TATκ-GFP-CDKL5₅ fusion protein

with a TATκ-CDKL5₅ protein without GFP and with only a small 3xFLAG-tag at the C-terminus (Supplementary Material Fig. S1, S2C). We found a similar effect on SH-SY5Y neuroblastoma cells in terms of inhibition of proliferation, indicating that the GFP-tag does not affect CDKL5 activity (Supplementary Material Fig. S2C). Treatment with the kinase-dead form of CDKL5 (TATκ-GFP-CDKL5(K42R)₁, Fig. 2B) did not affect SH-SY5Y cell proliferation, indicating that the TATκ-GFP-CDKL5 fusion proteins had preserved the kinase activity.

It has been shown that in neurons CDKL5 has mainly a cytoplasmic localization with an enrichment at the level of dendritic spines (6). To assess whether the transduced TATκ-GFP-CDKL5 localizes as the native form, we treated hippocampal neuronal cultures from *Cdkl5* KO male (-/Y) mice with purified TATκ-GFP-CDKL5₁, or TATκ-GFP (added to the culture medium). While transduced TATκ-GFP-CDKL5₁ located mainly at the nuclear level in astrocytes (Supplementary Material Fig. S3A), we found that in hippocampal neurons internalized TATκ-GFP-CDKL5₁ was distributed in the cytoplasmic compartment and, at a dendritic level, it was distributed in a manner that suggested a spine localization (Fig. 1D, Supplementary Material Fig. S3B). Confocal images showed TATκ-GFP-CDKL5₁ co-localization with the postsynaptic density protein PSD-95 (Fig. 2E) and with the presynaptic protein synaptophysin (SYN; Fig. 2E), suggesting that the exogenous protein localizes at the same postsynaptic level (i.e., dendritic spines) as the native CDKL5. Similar results were obtained with TATκ-GFP-CDKL5₅ (data not shown). In contrast, the control GFP protein (TATκ-GFP) showed a widespread distribution along the dendrites (Fig. 1D, Supplementary Material Fig. S4A).

In order to confirm the wild type activity of the recombinant proteins, hippocampal neuronal cultures from *Cdkl5* -/Y mice were grown in the presence of TATκ-GFP-CDKL5₁ or TATκ-GFP. Confirming previous evidence (14), the absence of *Cdkl5* caused a reduction in neuronal maturation, as shown by the reduced dendritic length (Fig. 2F,I; Supplementary Material Fig. S4B), number of synaptic terminals (SYN; Fig. 2G,I) and spine density (Fig. 2H,I; Supplementary Material Fig. S4C) (14). Treatment with TATκ-GFP-CDKL5₁ restored these defects (Fig. 2D-I; Supplementary Material Fig. S4B,C), confirming that the CDKL5 fusion protein retains physiological activity. Similar results on neuronal maturation were obtained with the TATκ-GFP-CDKL5₅ isoform (data not shown). As expected, treatment with the kinase-dead form of CDKL5 (TATκ-GFP-CDKL5(K42R)₁) had no effect on neuronal maturation (Fig. 2F-I, Supplementary Material Fig.

S4B).

Intracerebroventricular treatment with TATκ-CDKL5 protein improves behavior in *Cdkl5* KO mice

For the *in vivo* study, we decided to use TATκ-GFP-CDKL5₁ because it is the most-expressed isoform in the central nervous system (22) and shows comparable activity to the TATκ-GFP-CDKL5₅ isoform. As a control for the *in vivo* treatment, we used a TATκ-GFP fusion protein, since it has been shown that GFP does not influence cellular functions. In a first set of experiments we tested the efficacy of TATκ-GFP-CDKL5₁ following intracerebroventricular injections. We found that TATκ-GFP-CDKL5₁ and TATκ-GFP fusion proteins, infused directly to the lateral ventricle, diffused into the brain (Supplementary Material Fig. S5A), reaching the hippocampus (Supplementary Material Fig. S5B) and deeper brain structures (data not shown). Double immunofluorescence staining with an anti-GFP antibody and an anti-NeuN or anti-GFAP antibodies shows uptake by brain cells (neurons and astrocytes) of the injected protein (Supplementary Material Fig. S5C). Subcellular localization of transduced protein showed TATκ-GFP-CDKL5₁ co-localization with the postsynaptic density protein PSD-95, indicating a spine localization.

Cdkl5 KO (-/Y) mice received a single daily injection for 5 consecutive days, followed by a two-day rest period and then 5 additional days of a single injection, for a total of 10 injections (Fig. 3A). At the end of the treatment, animals were behaviorally tested during a 10-day period and sacrificed after testing (Fig. 3A). No changes in terms of body weight (Supplementary Material Fig. S6A) or sleep pattern (Supplementary Material Table S1) were observed in treated *Cdkl5* -/Y mice, indicating that TATκ-GFP-CDKL5₁ treatment does not affect these aspects of animal health. Moreover, treatment did not cause activation of microglial cells, evaluated using Allograft Inflammatory Factor 1 (AIF-1) staining (Supplementary Material Fig. S6B,C), indicating an absence of inflammatory response to continuous TATκ-GFP-CDKL5₁ treatment.

First, we evaluated behavioral improvement due to TATκ-GFP-CDKL5₁ treatment by focusing on the hippocampus, which is known to be severely impaired in *Cdkl5* -/Y mice at a functional level (10, 13, 27). To this aim, we used the Morris Water Maze (MWM) and Passive Avoidance (PA) tests. *Cdkl5* KO mice exhibit severe deficits for both these tasks (13, 14). In the MWM test, no learning improvement was detected in TATκ-GFP-treated *Cdkl5* -/Y mice compared to their untreated counterparts (Fig. 3B), indicating no effect of the control protein. Importantly, TATκ-GFP-CDKL5₁-treated *Cdkl5* -/Y mice underwent an improvement in their learning ability starting from day 3 and reaching a performance similar to that of

control (+/Y) mice on day 5 (Fig. 3B). In the probe trial, the latency to find the hidden platform was severely impaired in untreated and TATκ-GFP-treated *Cdkl5* -/Y mice (Fig. 3C). TATκ-GFP-CDKL5₁-treated *Cdkl5* -/Y mice showed a statistically significant improvement in memory performance (Fig. 3C). In the PA test, all groups showed similar step-through latencies on the first day (Fig. 3D). After 24 h, untreated and TATκ-GFP-treated *Cdkl5* -/Y mice were severely impaired in performing this task, as demonstrated by a reduced latency to enter the dark compartment in comparison with control (+/Y) mice. In contrast, TATκ-GFP-CDKL5₁-treated *Cdkl5* -/Y mice showed a similar latency as untreated +/Y mice, indicating memory restoration (Fig. 3D).

Using whole-body plethysmography (WBP), we recently found that sleep apneas occur more frequently in *Cdkl5* -/Y than in control (+/Y) mice (28) (Fig. 3F), indicating a breathing disturbance during sleep in *Cdkl5* -/Y mice. Though the sleep apnea occurrence rate of TATκ-GFP-treated *Cdkl5* -/Y mice resulted to be slightly lower compared to untreated *Cdkl5* -/Y mice, probably due to a minor stress response resulting from habituation to the prolonged handling (29), treatment with TATκ-GFP-CDKL5₁ led to a drastic reduction in the number of apneas, that became similar to that of control mice (+/Y) (Fig. 3E, F).

Finally, in order to examine the effect of TATκ-GFP-CDKL5₁ on motor stereotypies, mice were tested for hind-limb claspings before and after the 10 days of treatment (Fig. 3G). While +/Y mice exhibited no hind-limb claspings, *Cdkl5* -/Y mice spent about 1/4 of the test session in the claspings position (Fig. 3G). A similar claspings duration was observed in *Cdkl5* -/Y mice after treatment with TATκ-GFP (Fig. 3G). In contrast, *Cdkl5* -/Y mice treated with TATκ-GFP-CDKL5₁ showed a significant decrease in claspings (Fig. 3G), indicating a treatment-induced improvement of motor stereotypies.

These data show that CDKL5 replacement positively impacts on numerous behavioral deficits due to loss of *Cdkl5* expression.

Intracerebroventricular treatment with TATκ-CDKL5 protein restores dendritic abnormalities in *Cdkl5* KO mice

In order to establish whether the improvement of behavioral performance is due to a recovery of the brain structural defects that characterize *Cdkl5* KO mice (10, 12, 13, 27), we analyzed dendritic morphology

and connectivity in the hippocampus of *Cdkl5* ⁻/_Y mice that were treated according to the schedule shown in Fig. 3A and sacrificed ten days after the last intracerebroventricular injection.

The hippocampal dentate gyrus (DG) exhibits ongoing neurogenesis throughout life. The new granule neurons express doublecortin (DCX) from 1 to 4 weeks after neuron birth (30). We took advantage of this feature to examine the effect of treatment on neurons born shortly before, during the treatment, and in the 10 day period followed the beginning of treatment. As previously reported (12), DCX-positive granule cells of *Cdkl5* ⁻/_Y mice exhibit a shorter dendritic length in comparison with their wild type (+/Y) counterparts (Fig. 4A,B). Treatment with TATκ-GFP-CDKL5₁ increased total dendritic length in *Cdkl5* ⁻/_Y mice to levels similar to those of wild type mice (Fig. 4A,B). Treatment with TATκ-GFP had no effect on dendritic length (Fig. 4A,B). These data, taken together, show that replacement of CDKL5 is able to restore dendritic development.

Previous evidence showed that neurons of *Cdkl5* KO mice are characterized by severe dendritic pathology in terms of dendritic architecture and spine density (13). In order to establish whether treatment is able to reshape the dendritic pattern of neurons born well before treatment, in Golgi-stained brain sections (Fig. 4C) we examined the dendritic tree of granule cells of the DG and pyramidal neurons of hippocampal field CA1. Granule neurons of *Cdkl5* ⁻/_Y mice displayed reduced dendritic length (Fig. 4D,E) in comparison with wild type (+/Y) mice, due to a reduction of the number of branches (Fig. 4G), with no differences in the mean branch length (Fig. 4F). While dendritic length and number of branches were completely rescued by treatment with TATκ-GFP-CDKL5₁, treatment with TATκ-GFP had no effect (Fig. 4D,E,G). Similarly to granule neurons, pyramidal neurons of field CA1 (Fig. 4H) exhibited dendritic hypotrophy at the level of both the apical and basal dendritic trees (Fig. 4I). While treatment with TATκ-GFP did not affect the dendritic arbors of pyramidal neurons, treatment with TATκ-GFP-CDKL5₁ restored total dendritic length (Fig. 4I). These results show that CDKL5 replacement can restore the dendritic length of mature neurons and of neuronal populations in different hippocampal regions.

Evaluation of dendritic spine density showed that both the granule cells of the DG and CA1 pyramidal neurons had a reduced spine density in untreated *Cdkl5* ⁻/_Y mice in comparison with wild type (+/Y) mice (Fig. 5A-D). *Cdkl5* ⁻/_Y mice treated with TATκ-GFP-CDKL5₁ underwent restoration of spine density in both neuron types (Fig. 5A-D). Dendritic spines are heterogeneous in size and shape, and can be

classified as: immature spines (filopodia, thin-shaped and stubby-shaped) and mature spines (mushroom and cup shapes) (see Fig. 5B). Separate counts of different classes of dendritic spines revealed that the granule cells of *Cdkl5* ⁻/_Y mice had a higher percentage of immature spines and a reduced percentage of mature spines compared to ⁺/_Y mice (Fig. 5C). A similar imbalance was found in CA1 pyramidal neurons (Fig. 5D). Treatment with TATκ-GFP-CDKL5₁, but not with TATκ-GFP, largely improved the balance between immature and mature spines in both neuron types (Fig. 5C,D).

Most excitatory synapses in the mature mammalian brain occur on spines in which postsynaptic density protein 95 (PSD-95) clusters are localized (31). Evaluation of PSD-95 immunoreactivity showed that *Cdkl5* ⁻/_Y mice displayed a strong reduction in the number of PSD-95-positive puncta in the molecular layer of the DG (Fig. 5E,F). Treatment with TATκ-GFP-CDKL5₁ restored the number of PSD-95-positive puncta (Fig. 5E,F), which is consistent with the recovery of the mature spine number (Fig. 5C).

These results indicate that CDKL5 replacement restores the hippocampal structural defects that characterize *Cdkl5* KO mice with an effect that extends beyond the cessation of treatment.

Systemically-injected TATκ-CDKL5 protein reaches the mouse brain

In a second set of experiments, we sought to establish whether systemically-injected TATκ-GFP-CDKL5 protein crosses the blood brain barrier. This is an essential step for development of a CDKL5 protein substitution protocol suitable for clinical application. Since the blood brain barrier increases its selectivity with age, we evaluated whether TATκ-GFP-CDKL5 protein crosses the blood brain barrier in newborn and adult mice (Fig. 6A-D; Supplementary Material Fig. S7A,B). Seven-day old pups were subcutaneously injected with TATκ-GFP-CDKL5₁, TATκ-GFP-CDKL5₅, TATκ-GFP or vehicle (negative control) and sacrificed 4 h after the injection (Fig. 6A,B; Supplementary Material Fig. S7A). The localization of the TATκ-GFP-CDKL5₁, TATκ-GFP-CDKL5₅ and TATκ-GFP proteins in the brain was evaluated by immunohistochemistry, using an anti-GFP antibody. We found the presence of the TATκ-GFP-CDKL5 and TATκ-GFP proteins in the brain of mouse pups 4 h after the protein injection (Fig. 6B; Supplementary Material Fig. S7A). To assess whether the TATκ-GFP-CDKL5 protein crosses the highly selective permeability barrier of the adult brain, P90 mice were intravenously injected (a procedure that is feasible in adult mice) with TATκ-GFP-CDKL5 and sacrificed 1 h later (Fig. 6C,D; Supplementary Material Fig. S7B).

As shown in Fig. 6D, the TATκ-GFP-CDKL5₁ protein was distributed in the brain. These data demonstrate that TATκ-GFP-CDKL5 protein is effectively transported across both the “immature” and “mature” blood brain barrier.

Effect of systemically-administered TATκ-CDKL5 protein on dendritic morphology and behavior

We used an infusion method which is based on a programmable pump (IPRECIO, Primetech, Japan) implanted under the skin with a refillable reservoir. The pump was connected to a catheter implanted in the carotid artery. In view of the turnover of the TATκ-GFP-CDKL5₁ (see preceding sections), we decided to use a twice-a-day infusion protocol (bolus delivered at 9 am and 9 pm; see Methods for details) for the duration of 10 days (Fig. 7A). Mice were behaviorally tested from day 8 to day 12 and a separate cohort of animals were sacrificed on day 10 for histological analysis. Similarly to intracerebroventricular treatment, no changes in terms of body weight (Supplementary Material Fig. S8A) or sleep pattern (Supplementary Material Table S1) were observed in *Cdkl5* ^{-/-} mice that had undergone systemic administration of TATκ-GFP-CDKL5₁.

In order to establish whether systemic administration of TATκ-GFP-CDKL5₁ had positive effects on the dendritic hypotrophy of hippocampal neurons, we examined both newborn and mature granule cells. We found that, unlike TATκ-GFP-treated *Cdkl5* ^{-/-} mice, *Cdkl5* ^{-/-} mice treated with the TATκ-GFP-CDKL5₁ underwent restoration of total dendritic length of DCX-positive neurons (newborn granule cells) (Fig. 7B,C) as well as Golgi-stained granule cells (mature neurons) (Fig. 7D). Moreover, *Cdkl5* ^{-/-} mice treated with TATκ-GFP-CDKL5₁ underwent restoration of granule cell spine density (Fig. 7E).

Since we could not examine the effect of treatment on learning and memory with the MWM test because this test requires a motility in the water that would have been hampered by the weight and size of the implanted pump, learning and memory was evaluated using the Barnes maze. We found that, while untreated and TATκ-GFP-treated *Cdkl5* ^{-/-} mice took longer to locate the target hole compared to control mice, TATκ-GFP-CDKL5₁-treated *Cdkl5* ^{-/-} mice underwent an improvement in their learning ability (Fig. 7F). In the probe trial, the latency to find the target hole was severely impaired in untreated and TATκ-GFP-treated *Cdkl5* ^{-/-} mice (Fig. 7F). TATκ-GFP-CDKL5-treated *Cdkl5* ^{-/-} mice showed a similar improvement in latency to find the hole (Fig. 7F), indicating an effect of the protein therapy on memory performance.

We further examined digging and nesting, two spontaneous home-cage social behaviors that are associated with autistic-like phenotypes (32-34). In both tests, untreated as well as TATκ-GFP-treated *Cdkl5* -/Y mice exhibited an impaired performance compared to control (+/Y) mice. They showed reduced digging episodes and poorer or no nest-building compared to control (+/Y) mice (Fig. 7G,H). Digging and nesting behaviors were corrected by the TATκ-GFP-CDKL5₁ protein treatment (Fig. 7G,H), indicating a positive effect of the treatment on these spontaneous social behaviors.

Cdkl5 -/Y mice showed elevated locomotor activity and stereotyped behavior (repetitive vertical jumping (35)) in an open field compared to wild type littermate controls (Fig. 7I,J). *Cdkl5* -/Y mice moved at a higher average velocity (Fig. 7I), traveled a significantly longer distance (Fig. 7I), and showed an increased number of vertical stereotyped jumps (Fig. 7J). A similar elevated locomotor activity and stereotyped behavior was observed in *Cdkl5* -/Y mice after treatment with TATκ-GFP (Fig. 7I,J). In contrast, *Cdkl5* -/Y mice treated with TATκ-GFP-CDKL5₁ showed a significant decrease in hyperactivity (Fig. 7I) and motor stereotypies (Fig. 7J), indicating a treatment-induced improvement of autistic-like behaviors.

Effect of systemically-administered TATκ-CDKL5 protein on breathing pattern and cortical visual responses

Since impaired breathing pattern, particularly during sleep, and visual responses represent promising biomarkers for preclinical and clinical studies on CDKL5 disorder (28, 36), we evaluated the effect of the treatment with TATκ-GFP-CDKL5₁ or TATκ-GFP proteins on these two patterns in *Cdkl5* KO mice. In order to assess the long-lasting effect of the treatment, *Cdkl5* -/Y mice were tested on the tenth day of treatment and after 5 and 10 days after the end of treatment (Fig. 8A).

We found that, unlike TATκ-GFP treatment, 10 days of treatment with TATκ-GFP-CDKL5₁ led to a significant reduction in the occurrence rate of REM sleep apneas in *Cdkl5* -/Y mice (Fig. 8B). The positive effect of the TATκ-GFP-CDKL5₁ treatment on sleep apneas gradually disappeared 5-10 days after treatment cessation (Fig. 8B).

Cortical visual responses were assessed using non-invasive transcranial intrinsic optical signal (IOS) imaging, a method that allows us to monitor the visually-evoked responses in the same animal at different time points (36). We found that, while TATκ-GFP treated *Cdkl5* -/Y mice showed no improvement in visual

responses compared to the baseline condition (Fig. 8C,D), *Cdkl5*^{-/-} mice treated with the TAT κ -GFP-CDKL5₁ protein underwent a progressive restoration of visual responses that fell within the 95% confidence interval of wild-type mice (Fig. 8C,D). The positive effect of the TAT κ -GFP-CDKL5₁ protein treatment on visual response was retained 5-10 days after treatment cessation (washout), indicating a long-lasting effect of the protein replacement treatment.

In order to establish whether the improvement of visual performance of treated *Cdkl5*^{-/-} mice is associated with recovery of the defective synaptic organization that characterizes the primary visual cortex (V1) of *Cdkl5*^{-/-} mice (16), we analyzed spine density of layer II/III pyramidal neurons (Fig. 8E, Supplementary Material Fig. S8B). While untreated and TAT κ -GFP-treated *Cdkl5*^{-/-} mice showed a lower spine density compared to control (+/Y) mice (Fig. 8E), mice treated with TAT κ -GFP-CDKL5₁ underwent an increase in spine density (Fig. 8E). This effect was present at the end of treatment (short-term effect) and, albeit to a lesser extent, 10 days after treatment cessation (long-term effect). Evaluation of the number of PSD-95 immunoreactive puncta showed that, consistent with previous evidence (16), *Cdkl5*^{-/-} mice displayed a strong reduction in the number of PSD-95-positive puncta in layers II/III of V1 compared to control (+/Y) mice (Fig. 8F). Treatment with TAT κ -GFP-CDKL5₁ restored the number of PSD-95-positive puncta at treatment cessation (short-term, Fig. 8F) and this effect was retained 10 days after treatment cessation (long-term, Fig. 8F), which is consistent with the effect of treatment on spine density (Fig. 8E).

DISCUSSION

No therapies are presently available for the improvement of the neurological phenotypes associated with CDKL5 disorder. Since mutations in the *CDKL5* gene lead to a lack of functional CDKL5, delivery of a functional CDKL5 protein to the brain may represent a therapeutic approach of choice. Our study provides novel evidence that a protein substitution therapy, aimed at compensating for the lack of CDKL5 function, is feasible and effective. To deliver an active CDKL5 protein into the brain and within brain cells, we constructed the TAT κ -CDKL5 fusion protein using the HIV protein transduction domain TAT as a delivering moiety. We demonstrated that TAT κ -CDKL5 fusion protein is internalized by cells and retains

CDKL5 activity. When injected *in vivo*, TATκ-CDKL5 fusion protein was able to cross the blood-brain barrier and diffuse into brain cells. *Cdkl5*KO mice treated with TATκ-CDKL5 protein underwent a neurodevelopmental and behavioral improvement or even rescue. These promising results suggest that a protein substitution therapy with a TATκ-CDKL5 fusion protein may be a successful therapy for CDKL5 disorder. Moreover, our data represents the first successful attempt to use systemic protein replacement therapy for a neurodevelopmental disorder.

It is possible to create a functional TATκ-CDKL5 fusion protein

The results of initial studies in the field of protein therapy technology led to anticipation that it would soon be possible to develop fusion proteins for different brain diseases. However, it turned out that expression and purification of fusion proteins have methodological limitations. For instance, unsuccessful cell transduction has been described for a number of fusion constructs, including linking the TAT-PTD with diphtheria toxin A (37), with *Leishmania* gp63 (38) or with aromatic carboxylic acid (39). In the present study, we succeeded in producing a functional TATκ-CDKL5 fusion protein with cell transduction properties. As previously reported, CDKL5 protein cannot be produced in bacteria due to its massive degradation in prokaryotes(40). Conversely, we found that production of TATκ-CDKL5 in mammalian expression systems is feasible. In order to optimize production yields we created an Igκ-TATκ-CDKL5 fusion construct. In view of the properties of the Igκ-chain leader sequence polypeptide (25), the TATκ-CDKL5 fusion protein produced by the infected cells can be secreted via constitutive secretory pathways. Importantly, due to the transduction properties of the TATκ peptide, the secreted TATκ-CDKL5 fusion protein is efficiently internalized by target cells. When internalized, the TATκ-CDKL5 protein retains the wild-type CDKL5 activity, as demonstrated by its ability to inhibit neuroblastoma cell proliferation(26) and restore maturation of hippocampal neurons that lack CDKL5 expression (14). It is important to observe that CDKL5, being a high weight protein, may be liable to undergo conformational modification during the process of purification. Our results show that it is possible to create a fusion protein that retains functional activity even for a high-weight protein like CDKL5, demonstrating that it is possible to overcome the limitations posed by high-weight proteins in the field of protein therapy.

Therapeutic benefits of *in vivo* protein therapy

CDKL5 KO mice exhibit severe defects in the hippocampal region in terms of dendritic arborization, spine density, and pattern, and show a poorer performance in hippocampus dependent memory and learning tasks compared to wild-type mice (10, 12-14). The current study shows that a 10-day intraventricular treatment with TAT κ -CDKL5 restored maturation of hippocampal neurons in terms of dendritic arbor and spine density. Importantly, hippocampus-dependent behaviors of *Cdkl5* KO mice were significantly improved, indicating that the recovery of hippocampal structure in treated *Cdkl5* KO mice was functionally effective. Since behavioral testing was carried out during a 10-day period that followed treatment cessation, and assessment of dendritic arborization and spine density were carried out 10 days after treatment cessation, this suggests that the effects of TAT κ -CDKL5 protein treatment are retained (at least for 10 days) after treatment cessation. Protein treatment with TAT κ -CDKL5 fusion protein also reduces sleep apnea occurrence and stereotyped behavior (hind-limb clasping) in *Cdkl5* KO mice.

Since a therapy based on intracerebroventricular infusion in human beings is not feasible, we sought to establish whether TAT κ -CDKL5 protein administered systemically crosses the blood-brain barrier. We found that this was the case and that vascular infusion of TAT κ -CDKL5 led to restoration of neuroanatomical and behavioral defects in *Cdkl5* KO mice. Since visual function is notably impaired in children with CDKL5 disorder and in *Cdkl5* KO mice (36, 41-43), we examined the effect of systemic treatment on the primary visual cortex. (36). The longitudinal monitoring of the treatment showed that after 10 days of treatment visual responses had recovered in mice treated with TAT κ -CDKL5 fusion protein, whereas mice treated with control protein had no improvement. Both visual function amelioration and improvement of spine density and PSD-95 puncta staining outlasted the period of treatment, suggesting that discontinuous protocols of treatment could be effective. On the other hand, the restoration of sleep apnea occurrence due to systemic TAT κ -CDKL5 fusion protein administration did not persist beyond treatment cessation, suggesting that complex behaviors such as sleep breathing require closer or continuous treatments.

Our finding that TAT κ -CDKL5 is transduced in the brain by both neuronal and glial cells is in line with the nature of the TAT peptide to enter various cell types in a non-selective manner (44). Although at the moment the CDKL5 function is primarily imputable to its action at the neuronal level, we cannot rule out the

possibility that the re-introduction of CDKL5 into non-neuronal cells may partially underlie the behavioral improvement of TATκ-CDKL5-treated *Cdkl5* KO mice.

Recent studies have shown that various TAT fusion proteins are safe and efficiently transported in vitro and in vivo (45-48). A good example is Tat-NR2B9c, an inhibitor of postsynaptic density-95 protein, which has been demonstrated to safely and efficiently reduce ischemic brain damage in cynomolgus macaques and human beings (49, 50). After 10 days of TATκ-CDKL5 protein administration we did not observe evident side effects in terms of body weight or sleep pattern in *Cdkl5* KO mice. Assessment of the development of an immune response against therapeutic proteins may represent a critical issue. Regarding this issue, it is important to observe that we found no local inflammatory response after 10 days of treatment, suggesting an absence of immunogenicity problems regarding either the TAT-PTD or the CDKL5 protein. Further investigations are needed in order to establish whether a more prolonged treatment induces side effects.

Taken together, these findings suggest that a TATκ-CDKL5 protein therapy i) is feasible *in vivo*; ii) positively impacts on different brain functions; iii) has no adverse effects.

Conclusions

To date no cure is available for CDKL5 disorder and the standard of care for patients only targets specific symptoms (3). Very recently, pharmacological treatments targeting different signaling pathways were shown to be able to rescue various aspects of brain development in a *Cdkl5* KO mouse model (13, 14, 51). Mutations of CDKL5 are the upstream cause of all the molecular alterations characterizing CDKL5 disorder. Since the only common feature that is certainly shared by all CDKL5 patients is the lack of a functional CDKL5 protein, compensation of this defect with a protein therapy should theoretically restore all the reversible alterations in CDKL5 patients. Protein replacement therapy is commercially available for various lysosomal storage diseases and represents a potentially exciting avenue for other inherited enzyme deficiency disorders that currently lack available treatments (52-55). Importantly, several compounds involving PTDs have been tested in humans with no serious adverse effects (56). To the best of our knowledge, no PTD-tagged proteins have yet entered human clinical trials for brain disorders. Our study demonstrates the feasibility and efficacy of using a TATκ-CDKL5 protein as a therapeutic agent in an

experimental CDKL5 disease model. It is important to mention that another two lines of *Cdkl5* KO mice have been reported (9, 11). *Cdkl5* KO mouse models show a very similar but not always consistent phenotype. Moreover, the deficiency of *Cdkl5* in mice does not lead to spontaneous seizures, a common clinical profile in CDKL5 disorder. Therefore, even if our results strongly suggest the potential impact of a TATκ-CDKL5 protein therapy for CDKL5 disorder, it remains to be established whether this therapy is equally effective in patients with CDKL5 disorder.

MATERIAL AND METHODS

Mouse Colony – *Cdkl5* KO mice were produced and karyotyped as previously described (10). *Cdkl5* -/Y mice and *Cdkl5* +/Y littermate control mice were used for all experiments. The day of birth was designed as postnatal day (P) zero and animals with 24 h of age were considered as one-day-old animals (P1). After weaning, mice were housed 3 to 5 per cage on a 12-h light/dark cycle in a temperature- (23°C) and humidity-controlled environment with food and water provided *ad libitum*. The animals' health and comfort were controlled by the veterinary service. Experiments were performed in accordance with the Italian and European Community law for the use of experimental animals and were approved by Bologna University Bioethical Committee. In this study, all efforts were made to minimize animal suffering and to keep the number of animals used to a minimum.

CDKL5 vectors - Human CDKL5₅ cDNA was kindly provided by Marsha Rich Rosner (University of Chicago) (57). Human CDKL5₁ cDNA was kindly provided by Nicoletta Landsberger (University of Milan) (23). The secretable vector pPTKGFP, containing Igκ-chain V-J2-C signal peptide and codifying for the TATκ-GFP-myc-6xHis protein was kindly provided by Mahvash Tavassoli (King's College, London) (25). TATκ-GFP-CDKL5₅ and TATκ-GFP-CDKL5₁ constructs were produced as follows: human CDKL5₅ and CDKL5₁cDNAs were amplified using the following primers: 5'-CCGCTCGAGCGAAGATTCCTAACATTGG-3' (forward for both isoforms), 5'-

CCGCTCGAGCGGACTTGCCCGTCAGTGCC-3' (reverse for CDKL5₅), 5'-CCGCTCGAGCGGACAAGGCTGTCTCTTTTAAATC-3' (reverse for CDKL5₁) and cloned into pPTKGFPXhoI site in frame with upstream GFP sequence and downstream myc sequence. TATκ-CDKL5₅ construct was produced as follows: human CDKL5₅ was amplified using the following primers: 5'-GCACCGGTGAAGATTCCTAACATTGG-3' (forward), 5'-CCGC-TCGAGCGGATCACTACTTGTGCATCGTCATCC-3' (reverse) and cloned into pPTKGFPAgeI/XhoI sites. TATκ-GFP-CDKL5(K42R)₁ construct was performed to generate the inactive kinase K42R through PCR using the following primers: Fw 5'-AAATTCAAGGACAGTGAAGAAAATG-3'; Rv 5'-CCTGATCGCCACAATTTCATG-3' and a high fidelity Herculanase II Fusion DNA Polymerase (Agilent Technologies, CA, USA). For a detailed diagram of the constructs see Supplementary Material Fig. S1.

Stable clones expressing fusion proteins - HEK293T cells were transfected with the following vectors: TATκ-GFP, TATκ-GFP-CDKL5₅ and TATκ-GFP-CDKL5₁ using Lipofectamine 3000 (Invitrogen) transfection reagent according to the manufacturer's instructions. After 3 days, cells were selected with 5 µg/ml puromycin. Selection medium was changed every 3-4 days and clones were picked after 3 weeks. Clones were analyzed for TATκ-GFP, TATκ-GFP-CDKL5₅ and TATκ-GFP-CDKL5₁ expression and successively for protein secretion in culture medium by Western blot analysis with an anti-GFP antibody (rabbit polyclonal anti-GFP, 1:1000, Thermo Fisher Scientific) or an anti-CDKL5 antibody (rabbit polyclonal anti-CDKL5, 1:500, Sigma-Aldrich).

Protein Purification and Concentration - HEK293T cell lines expressing TATκ-GFP, TATκ-GFP-CDKL5₅ and TATκ-GFP-CDKL5₁ were grown for 48 h in serum-free culture medium (Dulbecco's modified Eagle's medium supplemented with 2 mM of glutamine and antibiotics: penicillin, 100 U/ml; streptomycin, 100 µg/ml). The culture medium containing the secreted proteins was collected, centrifuged to pellet cell debris and filtered through 0,2 µm syringe filters. The culture medium was then transferred to Amicon Ultra Centrifugal Filters (Millipore) with 50 kDa molecular weight cut-off, and proteins underwent diafiltration according to the manufacturer's instructions.

Evaluation of protein transduction efficacy - Neuronal cell lines - SH-SY5Y neuroblastoma cells were seeded onto poly-D-lysine coated slides in 24-well plates. Twenty-four h after plating, medium was replaced with fresh DMEM with 10% FBS plus medium containing TATκ-GFP-CDKL5₅ protein (50 ng). Thirty minutes after treatment cells were gently washed with PBS 1X and fixed with a 4% paraformaldehyde solution for 20 min at room temperature and immunocytochemistry with an anti-GFP antibody (rabbit polyclonal anti-GFP, 1:1000, Thermo Fisher Scientific) was performed. Fluorescence images to confirm TATκ-GFP-CDKL5₅ localization inside target cells were acquired using a LEICA TCS SL confocal microscope. Images were taken with a 63X oil immersion objective lens at 0.4 μm intervals (Z-stack).

Primary hippocampal neurons - Primary hippocampal neuronal cultures were prepared from P1 *Cdkl5* ^{-/-} and *Cdkl5* ^{+/+} mice as previously described (14). Protein transduction efficacy was evaluated by Western blot analysis on 4-day (DIV4) differentiated hippocampal neurons from *Cdkl5* ^{-/-} mice treated for 1 h with concentrated medium containing TATκ-GFP-CDKL5₁ protein (50 ng). Cells were gently washed with PBS 1X and directly collected in 2X SDS-PAGE loading buffer and processed for Western blot analysis using an anti-CDKL5 antibody (rabbit polyclonal anti-CDKL5, 1:500, Sigma-Aldrich). Localization of transduced protein was evaluated on 10-day (DIV10) differentiated hippocampal neurons treated for 1 h either with TATκ-GFP or TATκ-GFP-CDKL5₁ protein (50 ng). Immunostaining was performed using the following antibodies: anti-GFP (rabbit polyclonal anti-GFP, 1:1000, Thermo Fisher Scientific), anti-CDKL5 (sheep polyclonal SA145, MRC PPU reagent and service, University of Dundee, UK), anti-synaptophysin (mouse monoclonal anti-SYN (clone SY38) 1:500, Merck Millipore, USA), anti-PSD-95 (mouse monoclonal anti-PSD-95, 1:1000, Abcam, Cambridge, UK), anti-microtubule-associated protein 2 (rabbit polyclonal anti-MAP2, 1:1000, Millipore), anti-glial fibrillary acidic protein (mouse monoclonal anti-GFAP, 1:400, Sigma), and β-tubulin III (rabbit polyclonal anti-TUBJ 1:100, Sigma). Nuclei were stained either with Hoechst-33342 or TO-PRO-3. Images were acquired using a Nikon Eclipse E600 microscope equipped with a Nikon Digital Camera DXM1200 ATI System (Nikon Instruments Inc., Melville, NY, USA) or a LEICA TCS SL confocal microscope (Leica Microsystems, Wetzlar, Germany). For protein localization images were taken with a 63X oil immersion objective lens at 1 μm intervals (Z-stack).

Determination of TATκ-GFP-CDKL5₁ fusion protein half-life - HEK293T cells were treated with concentrated DMEM medium containing TATκ-GFP-CDKL5₁ protein (50 ng). At different time points (3 h, 6 h, 10 h and 24 h) cells were collected in 2X SDS-PAGE loading buffer and processed for Western blot analysis using an anti-CDKL5 antibody (rabbit polyclonal anti-CDKL5, 1:500, Sigma-Aldrich). Densitometric analysis of digitized images was performed using Chemidoc XRS Imaging Systems and Image Lab™ Software (Biorad). The Half life of the TATκ-GFP-CDKL5₁ protein was assessed, starting from the densitometric analysis of the protein bands over time. Assuming that protein degradation follows first-order decay kinetics, the logarithm of the fraction of protein that remained over time was plotted versus time. The graph's slope was used to evaluate the degradation rate constant (K). Starting from K, the half-life ($t_{1/2}$) of the protein, defined as the time required for the protein to halve its quantity, was calculated using the following equation: $t_{1/2} = \ln 2/K$ (58).

Evaluation of mitotic index - SH-SY5Y cells were treated for 24 h with 50 ng of the listed proteins: TATκ-GFP; TATκ-GFP-CDKL5₁ or TATκ-GFP-CDKL5(K42R)₁. Cells were fixed with a 4% paraformaldehyde solution for 20 min at room temperature and stained with Hoechst-33342. The mitotic index was evaluated with the number of mitotic cells as a percentage of total cell number for each condition.

Effects of TATκ-GFP-CDKL5₁ on *Cdkl5* KO hippocampal neurons - For morphological analysis (dendritic length, spine density and synaptic innervation) primary hippocampal neuron cultures from P1 *Cdkl5* ^{-/-}Y and *Cdkl5* ^{+/+}Y mice were treated with TATκ-GFP-CDKL5₁ or TATκ-GFP-CDKL5(K42R)₁ protein (50 ng) on alternate days starting from day 2 after plating (DIV2). Cells were fixed at DIV10 and processed for immunofluorescent staining and morphological analysis as previously described (14). Briefly, dendrite length of microtubule-associated protein 2 (MAP2)-positive neurons was measured and quantified by tracing along each neuronal projection using the image analysis system Image Pro Plus (Media Cybernetics, Silver Spring, MD, USA). The starting point of a dendrite was defined as the point at the midline of the dendrite that intersected the curvature of the soma. For our measures, a protrusion emerging from the cell soma with all its branches was counted as a single dendrite. Fluorescence images to evaluate spine density (MAP2-positive dendritic protrusions) were acquired using a Leica TCS SL confocal 63x oil

immersion lens at 0.6 mm intervals at 1,024 x 1,024 pixels resolution with 1x zoom. The confocal microscope acquisition parameters were kept the same for all scans. Spine density was measured by counting the number of dendritic protrusions (spines) on both primary and secondary dendrites and expressed as the number of spines per 10 μ m of dendritic length. The degree of synaptic innervation was evaluated by counting the number of synaptic (SYN) puncta on proximal dendrites and expressed as the number of SYN puncta per μ m of dendritic length (14).

Animal treatments and surgery - Animals were randomly assigned to the different treatments.

Intracerebroventricular cannula implantation and injections – Adult *Cdkl5*^{-/-} mice (4 to 6 months old) were implanted under general anesthesia (2% isoflurane in pure oxygen) with an intracerebroventricular (ICV) guide cannula (diameter 22 G, C313G, Plastics One, USA). The following stereotaxic coordinates were used to place the tip of the cannula in the lateral ventricle: 0.6 mm posterior and 1.2 mm lateral to bregma, 2 mm depth from the bone surface. The cannula was cemented to the skull with dental cement (RelyXUnicem, 3M ESPE, Italy) and dental acrylic (Respal NF, Italy) and plugged with a fitting cap (C313DC Plastics One, USA). Analgesic (Carprofen 5 mg/kg) and antibiotic (12500 U.I./kg benzylpenicillinbenzathine + 5 mg/kg dihydrostreptomycinsulphate) were given subcutaneously to each mouse. After 7 days of recovery, mice were anesthetized and an internal cannula (diameter 26 G, C312I, Plastics One, USA) connected to a Hamilton syringe was inserted into the guide cannula. Ten μ l of TAT κ -GFP-CDKL5₁ or TAT κ -GFP dissolved in saline was injected at a flow rate of 1 μ l/min using an infusion pump (Harvard Apparatus, USA; approximately 60 ng/infusion). The treatment period consisted of a single daily injection (10 μ l injection, approximately 60 ng/injection) for 5 consecutive days, followed by a two day rest period and then 5 additional days of a single injection. Thus, a total of 10 injections were administered over a 12-day period. At the end of treatment, animals were behaviorally tested and sacrificed 10 days after treatment cessation. Mouse body weight was recorded before each injection. The correct cannula position was verified via ink injection (1-2 μ l) at sacrifice. For the evaluation of *in vivo* protein transduction efficiency and localization, intracerebroventricular injections with TAT κ -GFP, TAT κ -GFP-CDKL5₁, TAT κ -GFP-CDKL5₅ protein (200 ng) or vehicle were performed on adult *Cdkl5*^{-/-} mice (3 months old) as described above and animals were sacrificed 1 or 6 h after a single injection. *Subcutaneous injections* –

Seven-day-old mouse pups (P7) were subcutaneously injected with TATκ-GFP, TATκ-GFP-CDKL5₁, TATκ-GFP-CDKL5₅ (200 ng) or vehicle. Animals were sacrificed 4 h after the injection and brains were fixed for immunofluorescent staining. *Intravenous injections* – Adult mice *Cdkl5* ^{-/-} mice (3 months old) were anesthetized with isoflurane (2% in pure oxygen) and dilation of the tail veins was stimulated by placing the tail in a warmer environment (40°C water bath) for several minutes. TATκ-GFP, TATκ-GFP-CDKL5₁, TATκ-GFP-CDKL5₅ protein preparation (250 ng) or vehicle, in a total volume of 200 µl, was slowly injected into the tail vein. The needle was then removed and an ethanol swab was applied directly to the injection site for 5-10 seconds to stop any bleeding. Mice were sacrificed 1h after the injection. *IPRECIO pump implantation and infusions* – Catheters for mouse carotid artery (INSTECH lab, USA) were treated with Tridodecylmethylammonium chloride (TDMAC, Sigma Aldrich, Italy) and heparin (Vister, 5000 U.I./ml, Pfizer) solutions following the manufacturer's instructions to prevent blood clots and then connected to micro infusion refillable pumps (IPRECIO SMP-300, Primetech Corporation, Japan). Adult *Cdkl5* ^{-/-} mice (4 to 6 months old) were anesthetized with isoflurane (2% in pure oxygen), the tip of the catheter was inserted into the internal carotid artery (cranial direction) and the IPRECIO pump was placed subcutaneously on the back of the mouse. Analgesic (Carprofen 5 mg/kg) and antibiotic (12500 U.I./kg benzylpenicillinbenzathine + 5 mg/kg dihydrostreptomycinsulphate) were given subcutaneously to each mouse. The IPRECIO reservoir (130 µl) was filled either with TATκ-GFP-CDKL5₁ or TATκ-GFP, and a 10-day infusion protocol was programmed as followed: 2 daily (1 in the morning and 1 in the evening) boluses (20 µl each corresponding to 50 ng of protein) were administered at 10 µl/h with a low constant release (0.4 µl/h) during the rest of the day to prevent catheter occlusion. Every 2 or 3 days mice were briefly anesthetized to refill the IPRECIO reservoir (transdermal injection) with fresh solutions. For mice used in the study of hypnic and ventilator dysfunctions, after 10 days of drug administration (either TATκ-GFP-CDKL5₁ or TATκ-GFP) the pump reservoir was emptied and refilled with saline. Saline infusions lasted for 10 more days following the same administration protocol. For mice used in the open field test, after 10 days of drug administration, IPRECIO pumps were removed and the carotid catheter was closed with a fitting cap. New stitches were applied to the backs of the mice and new doses of analgesic and antibiotic were provided. For mice used in the evoked potential study, a long postoperative recovery period (2 weeks) was allowed between the IPRECIO pump implantation and the beginning of drug administration. During this period, each

IPRECIO reservoir was filled with saline and just 1 daily bolus (at 10 μ l/h for 1h) was administered with a low constant release (0.6 μ l/h) during the rest of the day. The 10-day infusion protocol of drug/vehicle solution was the same used for all the other mice, but it was then followed by 10 more days (washout period) during which saline was continuously administered (at 0.4 μ l/h).

Histological and immunohistochemistry procedures – Mice were deeply anesthetized with isoflurane (4% in pure oxygen), brains were removed and cut along the midline and fixed by immersion in 4% paraformaldehyde in 100mM phosphate buffer, pH 7.4. Brains were stored in fixative for 48 h, kept in 20% sucrose in phosphate buffer for an additional 24 h and then frozen with cold ice. All steps of sectioning, imaging, and data analysis were conducted blindly and performed by two different operators. Brains were cut with a freezing microtome into 30- μ m-thick coronal sections that were serially collected. One out of 12 sections from the hippocampal formation were used for immunohistochemistry for doublecortin (goat polyclonal anti-DCX Ab, 1:100, Santa Cruz Biotechnology, Inc.) or anti-PSD-95 (rabbit polyclonal anti-PSD-95 Ab, 1:1000, Abcam, Cambridge, UK) as previously described (12, 14), or for anti-Allograft inflammatory factor 1 (rabbit polyclonal anti-AIF1 Ab, 1:1000, Thermo Fisher Scientific, Inc.). One out of 6 sections from the visual cortex was used for immunohistochemistry for PSD-95. For brain penetration analyses brain sections were incubated overnight at 4°C with a primary anti-GFP antibody (rabbit polyclonal anti-GFP, 1:1000, Thermo Fisher Scientific) and for 2 h with an HRP-conjugated anti-rabbit secondary antibody (1:200, Jackson ImmunoResearch, West Grove, PE, USA). Detection was performed using the TSA Cyanine 3 Plus Evaluation Kit (Perkin Elmer). For co-localization analyses double-fluorescence immunohistochemistry was performed. Brain sections were incubated overnight at 4°C with a primary anti-Neuronal nuclear antigen (mouse monoclonal anti-NeuN Ab, 1: 250; Chemicon, Billerica, MA, USA), an anti-glial fibrillary acidic protein (mouse monoclonal anti-GFAP Ab, 1:400, Sigma) or an anti-PSD-95 (mouse monoclonal anti-PSD-95, 1:200, Abcam, Cambridge, UK). Sections were then incubated with a FITC conjugated anti-mouse IgG (1:200, Jackson ImmunoResearch) secondary fluorescent antibody and further processed for anti-GFP staining as described above.

Golgi staining – Brains were Golgi-stained using the FD Rapid Golgi Stain™ Kit (FD NeuroTechnologies, Inc.) as previously described (59).

Measurements – *Neuron sampling*: Series of sections across the whole rostro-caudal extent of the DG were used for reconstruction of DCX-positive and Golgi stained neurons. DCX-positive neurons were sampled in the inner part of the granular layer, close to the subgranular zone. The Golgi method casually impregnates a few neurons from among a given population and allows one to sample relatively isolated neurons. Golgi-stained neurons were sampled from the outer part of the granule cell layer and in CA1. The total number of DCX-sampled granule cells was 15-18 per animal and the number of sampled Golgi-stained granule cells and CA1 pyramidal neurons was 10-15 per animal. *Measurement of the dendritic tree*: Dendritic trees of DCX-positive granule cells, Golgi-stained granule cells and CA1 pyramidal cells were traced with dedicated software, custom-designed for dendritic reconstruction (Immagini Computer, Milan, Italy), interfaced with Image Pro Plus (Media Cybernetics, Silver Spring, MD, USA). The dendritic tree was traced live, at a final magnification of 500×, by focusing on the depth of the section. The operator starts with branches emerging from the cell soma and after having drawn the first parent branch goes on with all daughter branches of the next order in a centrifugal direction. At the end of tracing the program reconstructs the total dendritic length, the mean length of branches and the number of segments. *Synaptic terminals*: For quantification of PSD-95 immunoreactive synaptic puncta, images from the molecular layer of DG and the primary visual cortex (V1) were evaluated as previously described using a LEICA TCS SL confocal microscope (14). *Spine density/morphology* - In Golgi-stained sections, spines of granule neurons, CA1 pyramidal neurons, and pyramidal neurons in layers II/III of the primary visual cortex (V1) were counted using a 100× oil immersion objective lens. Dendritic spine density was measured by manually counting the number of dendritic spines and expressed as the number of dendritic spines per 10 µm dendritic length. The number of dendritic segments counted per animal was 10-15.

Behavioral testing – All animal behavioral studies were performed blinded to genotype or treatment. Mice were allowed to habituate to the testing room for at least 1 h before the test, and testing was performed at the same time of the day. The sequence of the tests was arranged to minimize the effect of one test influencing

subsequent evaluation of the next test. *Hippocampus-dependent learning and memory behavior* - Animals were tested in the Morris Water Maze (MWM) or the Barnes Maze (BM), and in the Passive Avoidance task (PA) as previously described (14, 60). For the MWM a visual cue test was conducted 30 min after the probe test to assess sensorimotor ability and motivation. For this test, the platform was set 1 cm above the water level and marked with a flag so that the mice could locate the platform using a local visual stimulus rather than relying on spatial orientation to extra-maze cues. Animals were excluded from the analysis if they floated in more than 75% of the trials for more than 20 seconds or failed the visual cue test. For the BM, mice were trained to locate the target hole (with an underneath escape box) from 20 holes (5 cm diameter) evenly spaced around the perimeter of an elevated (60 cm above the floor) circular open field (100 cm diameter) (Ugo Basile, Italy). The escape box was designated as an analog to the hidden platform in the MWM, containing a ramp under the target hole so that mice could enter the escape box easily. Mice were initially placed in the center of the arena covered by a dark cylinder, which was removed 10 seconds after the start of a trial. All mice were trained with three trials per day for 3 consecutive days with an inter-trial interval of 30 min. Mice that initially failed to locate the target hole within 3 min were gently guided to the target by the operator. The mouse was left in the escape box for 1 min and then returned to its home cage before the next training trial. On the next day mice were tested for the “probe trial”(trial duration 90 seconds) in which the escape box was removed. All training trials and probe trials were videotaped for 3 min and the latency to enter the escape box/target hole were automatically scored by EthoVision10XT software (Noldus, The Netherlands). *Hind-limb clasping* – Animals were suspended by their tail for 2 min and hind-limb clasping was assessed independently by two operators from video recordings. A clasping event is defined by the retraction of limbs into the body and toward the midline. *Nesting behavior* – Nest-building ability was evaluated as proposed by Deacon (61). Animals were placed in individual cages with standard bedding and a standard piece of paper towel (23cm x 23cm) was provided 20-24 h prior to evaluation. The nests were assessed independently by two operators using the following scoring system: 0-no nest, 1-primitive flat nest (pad-shaped, consist of a flat paper tissue which slightly elevates a mouse above the bedding), 2-more complex nest (including warping and biting the paper towel), 3-complex accurate cup-shaped nests (with shredded paper interwoven to form the walls of the cup), 4-complex hooded nest, with walls forming a ceiling so the nest becomes a hollow sphere with one opening. *Digging behavior* – The test was performed as

previously described (61). Briefly, mice were placed in a clean 36.5cm × 20.7cm × 14.0cm cage with approximately 5cm thick standard wooden bedding. After each test the bedding was flattened, firmed and reused. Test duration was 210s. The number of digging bouts was recorded. Digging was assessed independently by two operators and defined as coordinated movements of fore- or hind-limbs that displace the substrate. *Open Field* - To assess locomotion, animals, after removing the pump, were placed in the center of a square arena (50 x 50 cm) and their behavior was monitored for 20 min using a video camera placed above the center of the arena. Distinct features of locomotor activity, including total distance traveled and average locomotion velocity were scored using EthoVision10XT software (Noldus, The Netherlands). The number of stereotypical jumps (repetitive beam breaks < 1 s) were manually counted by a trained observer who was blind to genotype and treatment. Test chambers were cleaned with 70% ethanol between test subjects.

Non-invasive assessment of sleep and breathing pattern – Hypnic and respiratory phenotypes of *Cdkl5* -/Y mice were assessed non-invasively with a validated technique based on whole-body plethysmography (WBP) (28, 62). Briefly, each mouse was placed inside a WBP chamber flushed with air at 1.5 l/h for the first 8h of the light period. The respiratory (WBP chamber pressure) signal was continuously recorded, together with chamber humidity and temperature, digitized, and stored at 128 Hz, 4 Hz, and 4 Hz, respectively. The system was calibrated with a 100µl micro-syringe (Hamilton, Reno, USA) at the end of each recording. The states of wakefulness, non-rapid-eye-movement sleep (NREMS) and rapid-eye-movement sleep (REMS) were blindly scored based on inspection of the raw WBP signal. Quantitative analysis of breathing was restricted to stable sleep episodes ≥ 12s because of the frequent occurrence of movement artefacts during wakefulness. Apneas and augmented breaths (sighs) were automatically detected as breaths with T_{TOT} (apneas) or tidal volume (sighs) > 3 times the average T_{TOT} or tidal volume, respectively, for each mouse and sleep state, and detection accuracy was checked on raw recordings. Since we previously demonstrated that the occurrence rate of all sleep apneas is the best biomarker to discriminate *Cdkl5* -/Y from control mice (28), in the present study sleep apneas were not further categorized as post-sigh or spontaneous apneas. WBP recordings were performed both in mice treated with ICV injections and in mice implanted with IPRECIO pumps. For the evaluation of long-term effects

of drug treatment, in the latter group of mice WBP recordings were performed after 10 days of drug administration (either with TATκ-GFP-CDKL5₁ or TATκ-GFP) and were repeated after 5 and 10 more days during which saline was infused.

Assessment of visual responses – The methods employed in (36) were used. Adult *Cdkl5* ^{-/-} mice implanted with IPRECIO pumps were box-anesthetized and maintained with isoflurane (respectively, 3% and 1%), placed on a stereotaxic frame, and the head fixed in place using ear bars. Body temperature was controlled using a heating pad and a rectal probe to maintain the animal's body at 37°C. Local anesthesia was provided using subcutaneous lidocaine (2%) injection and eyes were protected with dexamethasone-based ointment (Tobradex, Alcon Novartis). The scalp was removed and the skull carefully cleaned with saline. Skin was secured to the skull using cyanoacrylate. Then a thin layer of cyanoacrylate was poured over the exposed skull to attach a custom-made metal ring (9 mm internal diameter) centered over the binocular visual cortex. When the glue dried, a drop of transparent nail polish was spread over the area to ameliorate optical access. After surgery, the animals were placed in a heated box and monitored to ensure the absence of any sign of discomfort. Before any other experimental procedure, mice were left to recover for at least 36 h. During this period, paracetamol (5 mg/ml) was administered in the water as an analgesic therapy. IOS recordings were performed under isoflurane anaesthesia (0.5-1%) supplemented with an intraperitoneal injection of Chlorprothixene hydrochloride (1.25 mg/Kg). Images were obtained using an Olympus microscope (BX50WI). Red light illumination was provided by 8 red LEDs (625 nm, Knight Lites KSB1385-1P) attached to the objective (Zeiss Plan-NEOFLUAR 5x, NA: 0.16) using a custom-made metal LED holder. The animal was secured under the objective using a ring-shaped neodymium magnet mounted on an arduino-based 3D printed imaging chamber that also controls eye shutters and a thermostated heating pad (30). Visual stimuli were generated using MatlabPsychtoolbox and presented on a gamma corrected 9.7 inch monitor, placed 10 cm away from the eyes of the mouse. Contrast reversing Gabor patches (temporal frequency: 4Hz, duration: 1s) were presented in the binocular portion of the visual field (-10° to +10° relative to the horizontal midline and -5° to +50° relative to the vertical midline) with a spatial frequency of 0.03 cycles per degree, mean luminance 20 cd/m² and a contrast of 90%. Visual stimulation was time locked with a 16 bit depth acquisition camera (Hamamatsu digital camera

C11440) using a parallel port trigger. Interstimulus time was 14 seconds. Frames were acquired at 30 fps with a resolution of 512x512 pixels, low-pass filtered with a 2D average spatial filter (30 pixels, $117 \mu\text{m}^2$ square kernel), and downsampled to 128x128 pixels. The signal was averaged for at least 120 trials and downsampled to 10 fps. Fluctuations of reflectance (R) for each pixel were computed as the normalized difference from the average baseline ($\Delta R/R$). For each recording, an image representing the mean evoked response was computed by averaging frames between 0.5 to 2.5 seconds after stimulation. A region of interest (ROI) was automatically calculated on the mean image of the response, by selecting pixels in the lowest 30% $\Delta R/R$ of the range between the maximal and minimal intensity value. Mean evoked responses were quantitatively measured as the average intensity inside the ROI. To weaken background fluctuations a manually-selected polygonal region of reference (ROR) was subtracted. The ROR was placed where no stimulus response, blood vessel artifact or irregularities of the skull were observed (36).

Statistical analysis - Data from single animals represented the unit of analysis. Results are presented as mean \pm standard error (SE). Data distribution was assessed using a Kolmogorov-Smirnov nonparametric test of equality. Differences among multiple means were assessed, as indicated, by one-way or repeated-measures ANOVAs followed by Fisher's LSD or Holm-Sidak's post-hoc analysis. Datasets with non-parametric distribution were analyzed using the Kruskal-Wallis test. Post hoc multiple comparisons were carried out using Dunn's multiple comparison test. Statistical analyses were performed with GraphPad Prism (version 6.0) or SPSS (version 23). A probability level of $p < 0.05$ was considered to be statistically significant.

FUNDING: This work was supported by grants to: E.C. from MiaMed and Amicus Therapeutics; E.C. and T.P. from Telethon (GGP15098); E.C. from Fondazione del Monte di Bologna e Ravenna; E.C. from the Italian parent Associations “CDKL5 associazione di volontariatoOnlus” and “CDKL5 insieme verso la cura”.

ACKNOWLEDGMENTS: We thank Prof. Franco Laccone for advice on fusion protein design, and Massimiliano Cont for technical support with intravenous injections. We thank Dr. Sean Clark, Amicus Therapeutics, for his careful reading of the manuscript.

CONFLICT OF INTEREST STATEMENT. The authors have declared that no conflict of interest exists.

REFERENCES

- 1 Mari, F., Azimonti, S., Bertani, I., Bolognese, F., Colombo, E., Caselli, R., Scala, E., Longo, I., Grosso, S., Pescucci, C. *et al.* (2005) CDKL5 belongs to the same molecular pathway of MeCP2 and it is responsible for the early-onset seizure variant of Rett syndrome. *Hum Mol Genet*, **14**, 1935-1946.
- 2 Bertani, I., Rusconi, L., Bolognese, F., Forlani, G., Conca, B., De Monte, L., Badaracco, G., Landsberger, N. and Kilstrup-Nielsen, C. (2006) Functional consequences of mutations in CDKL5, an X-linked gene involved in infantile spasms and mental retardation. *J Biol Chem*, **281**, 32048-32056.
- 3 Fehr, S., Wilson, M., Downs, J., Williams, S., Murgia, A., Sartori, S., Vecchi, M., Ho, G., Polli, R., Psoni, S. *et al.* (2013) The CDKL5 disorder is an independent clinical entity associated with early-onset encephalopathy. *Eur J Hum Genet*, **21**, 266-273.
- 4 Guerrini, R. and Parrini, E. (2012) Epilepsy in Rett syndrome, and CDKL5- and FOXP1-gene-related encephalopathies. *Epilepsia*, **53**, 2067-2078.
- 5 Chen, Q., Zhu, Y.C., Yu, J., Miao, S., Zheng, J., Xu, L., Zhou, Y., Li, D., Zhang, C., Tao, J. *et al.* (2010) CDKL5, a protein associated with rett syndrome, regulates neuronal morphogenesis via Rac1 signaling. *J Neurosci*, **30**, 12777-12786.
- 6 Ricciardi, S., Ungaro, F., Hambrock, M., Rademacher, N., Stefanelli, G., Brambilla, D., Sessa, A., Magagnotti, C., Bachi, A., Giarda, E. *et al.* (2012) CDKL5 ensures excitatory synapse stability by reinforcing NGL-1-PSD95 interaction in the postsynaptic compartment and is impaired in patient iPSC-derived neurons. *Nature cell biology*, **14**, 911-923.
- 7 Rusconi, L., Salvatoni, L., Giudici, L., Bertani, I., Kilstrup-Nielsen, C., Broccoli, V. and Landsberger, N. (2008) CDKL5 expression is modulated during neuronal development and its subcellular distribution is tightly regulated by the C-terminal tail. *J Biol Chem*, **283**, 30101-30111.
- 8 Zhu, Y.C., Li, D., Wang, L., Lu, B., Zheng, J., Zhao, S.L., Zeng, R. and Xiong, Z.Q. (2013) Palmitoylation-dependent CDKL5-PSD-95 interaction regulates synaptic targeting of CDKL5 and dendritic spine development. *Proc Natl Acad Sci U S A*, **110**, 9118-9123.
- 9 Wang, I.T., Allen, M., Goffin, D., Zhu, X., Fairless, A.H., Brodtkin, E.S., Siegel, S.J., Marsh, E.D., Blendy, J.A. and Zhou, Z. (2012) Loss of CDKL5 disrupts kinome profile and event-related potentials leading to autistic-like phenotypes in mice. *Proc Natl Acad Sci U S A*, **109**, 21516-21521.

- 10 Amendola, E., Zhan, Y., Mattucci, C., Castroflorio, E., Calcagno, E., Fuchs, C., Lonetti, G., Silingardi, D., Vyssotski, A.L., Farley, D. *et al.* (2014) Mapping pathological phenotypes in a mouse model of CDKL5 disorder *Plos One*, **9**, e91613.
- 11 Okuda, K., Kobayashi, S., Fukaya, M., Watanabe, A., Murakami, T., Hagiwara, M., Sato, T., Ueno, H., Ogonuki, N., Komano-Inoue, S. *et al.* (2017) CDKL5 controls postsynaptic localization of GluN2B-containing NMDA receptors in the hippocampus and regulates seizure susceptibility. *Neurobiol Dis*, **106**, 158-170.
- 12 Fuchs, C., Trazzi, S., Roberta, T., Viggiano, R., De Franceschi, M., E., A., Gross, C.T., Calzà, L., Bartesaghi, R. and Ciani, E. (2014) Loss of Cdk15 impairs survival and dendritic growth of newborn neurons by altering AKT/GSK-3beta signaling. *Neurobiology of Disease*, **doi: 10.1016/j.nbd.2014.06.006**.
- 13 Fuchs, C., Rimondini, R., Viggiano, R., Trazzi, S., De Franceschi, M., Bartesaghi, R. and Ciani, E. (2015) Inhibition of GSK3beta rescues hippocampal development and learning in a mouse model of CDKL5 disorder. *Neurobiol Dis*, **82**, 298-310.
- 14 Trazzi, S., Fuchs, C., Viggiano, R., De Franceschi, M., Valli, E., Jedynak, P., Hansen, F.K., Perini, G., Rimondini, R., Kurz, T. *et al.* (2016) HDAC4: a key factor underlying brain developmental alterations in CDKL5 disorder. *Hum Mol Genet*, in press.
- 15 Della Sala, G., Putignano, E., Chelini, G., Melani, R., Calcagno, E., Michele Ratto, G., Amendola, E., Gross, C.T., Giustetto, M. and Pizzorusso, T. (2016) Dendritic Spine Instability in a Mouse Model of CDKL5 Disorder Is Rescued by Insulin-like Growth Factor 1. *Biol Psychiatry*, **80**, 302-311.
- 16 Pizzo, R., Gurgone, A., Castroflorio, E., Amendola, E., Gross, C., Sassoe-Pognetto, M. and Giustetto, M. (2016) Lack of Cdk15 Disrupts the Organization of Excitatory and Inhibitory Synapses and Parvalbumin Interneurons in the Primary Visual Cortex. *Frontiers in cellular neuroscience*, **10**, 261.
- 17 Bolhassani, A., Jafarzade, B.S. and Mardani, G. (2017) In vitro and in vivo delivery of therapeutic proteins using cell penetrating peptides. *Peptides*, **87**, 50-63.

- 18 Xia, H., Mao, Q. and Davidson, B.L. (2001) The HIV Tat protein transduction domain improves the biodistribution of beta-glucuronidase expressed from recombinant viral vectors. *Nat Biotechnol*, **19**, 640-644.
- 19 Schwarze, S.R., Ho, A., Vocero-Akbani, A. and Dowdy, S.F. (1999) In vivo protein transduction: delivery of a biologically active protein into the mouse. *Science*, **285**, 1569-1572.
- 20 Nagahara, H., Vocero-Akbani, A.M., Snyder, E.L., Ho, A., Latham, D.G., Lissy, N.A., Becker-Hapak, M., Ezhevsky, S.A. and Dowdy, S.F. (1998) Transduction of full-length TAT fusion proteins into mammalian cells: TAT-p27Kip1 induces cell migration. *Nat Med*, **4**, 1449-1452.
- 21 Kilstrup-Nielsen, C., Rusconi, L., La Montanara, P., Ciceri, D., Bergo, A., Bedogni, F. and Landsberger, N. (2012) What we know and would like to know about CDKL5 and its involvement in epileptic encephalopathy. *Neural plasticity*, **2012**, 728267.
- 22 Hector, R.D., Dando, O., Landsberger, N., Kilstrup-Nielsen, C., Kind, P.C., Bailey, M.E. and Cobb, S.R. (2016) Characterisation of CDKL5 Transcript Isoforms in Human and Mouse. *PLoS One*, **11**, e0157758.
- 23 Williamson, S.L., Giudici, L., Kilstrup-Nielsen, C., Gold, W., Pelka, G.J., Tam, P.P., Grimm, A., Prodi, D., Landsberger, N. and Christodoulou, J. (2012) A novel transcript of cyclin-dependent kinase-like 5 (CDKL5) has an alternative C-terminus and is the predominant transcript in brain. *Hum Genet*, **131**, 187-200.
- 24 Katayama, S., Sueyoshi, N. and Kameshita, I. (2015) Critical Determinants of Substrate Recognition by Cyclin-Dependent Kinase-like 5 (CDKL5). *Biochemistry*, **54**, 2975-2987.
- 25 Flinterman, M., Farzaneh, F., Habib, N., Malik, F., Gaken, J. and Tavassoli, M. (2009) Delivery of therapeutic proteins as secretable TAT fusion products. *Mol Ther*, **17**, 334-342.
- 26 Valli, E., Trazzi, S., Fuchs, C., Erriquez, D., Bartesaghi, R., Perini, G. and Ciani, E. (2012) CDKL5, a novel MYCN-repressed gene, blocks cell cycle and promotes differentiation of neuronal cells. *Biochim Biophys Acta*, **1819**, 1173-1185.
- 27 Trazzi, S., Fuchs, C., Valli, E., Perini, G., Bartesaghi, R. and Ciani, E. (2013) The amyloid precursor protein (APP) triplicated gene impairs neuronal precursor differentiation and neurite

development through two different domains in the Ts65Dn mouse model for Down syndrome. *J Biol Chem*, **288**, 20817-20829.

28 Lo Martire, V., Alvente, S., Bastianini, S., Berteotti, C., Silvani, A., Valli, A., Viggiano, R., Ciani, E. and Zoccoli, G. (2017) CDKL5 deficiency entails sleep apneas in mice. *J Sleep Res*, in press.

29 Ren, J., Ding, X., Funk, G.D. and Greer, J.J. (2012) Anxiety-related mechanisms of respiratory dysfunction in a mouse model of Rett syndrome. *J Neurosci*, **32**, 17230-17240.

30 Couillard-Despres, S., Winner, B., Schaubeck, S., Aigner, R., Vroemen, M., Weidner, N., Bogdahn, U., Winkler, J., Kuhn, H.G. and Aigner, L. (2005) Doublecortin expression levels in adult brain reflect neurogenesis. *Eur J Neurosci*, **21**, 1-14.

31 Scannevin, R.H. and Huganir, R.L. (2000) Postsynaptic organization and regulation of excitatory synapses. *Nat Rev Neurosci*, **1**, 133-141.

32 Silverman, J.L., Yang, M., Lord, C. and Crawley, J.N. (2010) Behavioural phenotyping assays for mouse models of autism. *Nat Rev Neurosci*, **11**, 490-502.

33 Greco, B., Manago, F., Tucci, V., Kao, H.T., Valtorta, F. and Benfenati, F. (2013) Autism-related behavioral abnormalities in synapsin knockout mice. *Behav Brain Res*, **251**, 65-74.

34 Moretti, P., Bouwknecht, J.A., Teague, R., Paylor, R. and Zoghbi, H.Y. (2005) Abnormalities of social interactions and home-cage behavior in a mouse model of Rett syndrome. *Hum Mol Genet*, **14**, 205-220.

35 Tanimura, Y., Ogoegbunam, F.C. and Lewis, M.H. (2009) Amphetamine-induced sensitization and spontaneous stereotypy in deer mice. *Pharmacol Biochem Behav*, **92**, 670-675.

36 Mazziotti, R., Lupori, L., Sagona, G., Gennaro, M., Della Sala, G., Putignano, E. and Pizzorusso, T. (2017) Searching for biomarkers of CDKL5 disorder: early-onset visual impairment in CDKL5 mutant mice. *Hum Mol Genet*, **26**, 2290-2298.

37 Falnes, P.O., Wesche, J. and Olsnes, S. (2001) Ability of the Tat basic domain and VP22 to mediate cell binding, but not membrane translocation of the diphtheria toxin A-fragment. *Biochemistry*, **40**, 4349-4358.

38 Corradin, S., Ransijn, A., Corradin, G., Bouvier, J., Delgado, M.B., Fernandez-Carneado, J., Mottram, J.C., Vergeres, G. and Mauel, J. (2002) Novel peptide inhibitors of Leishmania gp63 based on

the cleavage site of MARCKS (myristoylated alanine-rich C kinase substrate)-related protein. *Biochem J*, **367**, 761-769.

39 Kramer, S.D. and Wunderli-Allenspach, H. (2003) No entry for TAT(44-57) into liposomes and intact MDCK cells: novel approach to study membrane permeation of cell-penetrating peptides. *Biochim Biophys Acta*, **1609**, 161-169.

40 Kameshita, I., Sekiguchi, M., Hamasaki, D., Sugiyama, Y., Hatano, N., Suetake, I., Tajima, S. and Sueyoshi, N. (2008) Cyclin-dependent kinase-like 5 binds and phosphorylates DNA methyltransferase 1. *Biochem Biophys Res Commun*, **377**, 1162-1167.

41 Moseley, B.D., Dhamija, R., Wirrell, E.C. and Nickels, K.C. (2012) Historic, clinical, and prognostic features of epileptic encephalopathies caused by CDKL5 mutations. *Pediatr Neurol*, **46**, 101-105.

42 Bahi-Buisson, N., Nectoux, J., Rosas-Vargas, H., Milh, M., Boddaert, N., Girard, B., Cances, C., Ville, D., Afenjar, A., Rio, M. *et al.* (2008) Key clinical features to identify girls with CDKL5 mutations. *Brain*, **131**, 2647-2661.

43 Paine, S.M., Munot, P., Carmichael, J., Das, K., Weber, M.A., Prabhakar, P. and Jacques, T.S. (2012) The neuropathological consequences of CDKL5 mutation. *Neuropathol Appl Neurobiol*, **38**, 744-747.

44 Brooks, H., Lebleu, B. and Vives, E. (2005) Tat peptide-mediated cellular delivery: back to basics. *Adv Drug Deliv Rev*, **57**, 559-577.

45 Gou, X., Wang, Q., Yang, Q., Xu, L. and Xiong, L. (2011) TAT-NEP1-40 as a novel therapeutic candidate for axonal regeneration and functional recovery after stroke. *J Drug Target*, **19**, 86-95.

46 Wang, Q., Gou, X., Jin, W., Xiong, L., Hou, L., Chen, S., Zhang, H., Zhu, X. and Xu, L. (2009) TAT-mediated protein transduction of Nogo extracellular peptide 1-40 and its biological activity. *Cell Mol Neurobiol*, **29**, 97-108.

47 Wang, Q., Gou, X., Xiong, L., Jin, W., Chen, S., Hou, L. and Xu, L. (2008) Trans-activator of transcription-mediated delivery of NEP1-40 protein into brain has a neuroprotective effect against focal cerebral ischemic injury via inhibition of neuronal apoptosis. *Anesthesiology*, **108**, 1071-1080.

- 48 Deng, B., Gou, X., Chen, H., Li, L., Zhong, H., Xu, H., Jiang, F., Zhao, Z., Wang, Q. and Xu, L. (2013) Targeted delivery of neurogenin-2 protein in the treatment for cerebral ischemia-reperfusion injury. *Biomaterials*, **34**, 8786-8797.
- 49 Hill, M.D., Martin, R.H., Mikulis, D., Wong, J.H., Silver, F.L., Terbrugge, K.G., Milot, G., Clark, W.M., Macdonald, R.L., Kelly, M.E. *et al.* (2012) Safety and efficacy of NA-1 in patients with iatrogenic stroke after endovascular aneurysm repair (ENACT): a phase 2, randomised, double-blind, placebo-controlled trial. *Lancet Neurol*, **11**, 942-950.
- 50 Cook, D.J., Teves, L. and Tymianski, M. (2012) A translational paradigm for the preclinical evaluation of the stroke neuroprotectant Tat-NR2B9c in gyrencephalic nonhuman primates. *Science translational medicine*, **4**, 154ra133.
- 51 Della Sala, G., Putignano, E., Chelini, G., Melani, R., Calcagno, E., Michele Ratto, G., Amendola, E., Gross, C.T., Giustetto, M. and Pizzorusso, T. (2015) Dendritic Spine Instability in a Mouse Model of CDKL5 Disorder Is Rescued by Insulin-like Growth Factor 1. *Biol Psychiatry*, in press.
- 52 Rapoport, M., Salman, L., Sabag, O., Patel, M.S. and Lorberboum-Galski, H. (2011) Successful TAT-mediated enzyme replacement therapy in a mouse model of mitochondrial E3 deficiency. *Journal of molecular medicine*, **89**, 161-170.
- 53 Lawlor, M.W., Armstrong, D., Viola, M.G., Widrick, J.J., Meng, H., Grange, R.W., Childers, M.K., Hsu, C.P., O'Callaghan, M., Pierson, C.R. *et al.* (2013) Enzyme replacement therapy rescues weakness and improves muscle pathology in mice with X-linked myotubular myopathy. *Hum Mol Genet*, **22**, 1525-1538.
- 54 Higuchi, K., Yoshimitsu, M., Fan, X., Guo, X., Rasaiah, V.I., Yen, J., Tei, C., Takenaka, T. and Medin, J.A. (2010) Alpha-galactosidase A-Tat fusion enhances storage reduction in hearts and kidneys of Fabry mice. *Mol Med*, **16**, 216-221.
- 55 Eavri, R. and Lorberboum-Galski, H. (2007) A novel approach for enzyme replacement therapy. The use of phenylalanine hydroxylase-based fusion proteins for the treatment of phenylketonuria. *J Biol Chem*, **282**, 23402-23409.
- 56 Verdurmen, W.P. and Brock, R. (2011) Biological responses towards cationic peptides and drug carriers. *Trends in pharmacological sciences*, **32**, 116-124.

- 57 Lin, C., Franco, B. and Rosner, M.R. (2005) CDKL5/Stk9 kinase inactivation is associated with neuronal developmental disorders. *Hum Mol Genet*, **14**, 3775-3786.
- 58 Belle, A., Tanay, A., Bitincka, L., Shamir, R. and O'Shea, E.K. (2006) Quantification of protein half-lives in the budding yeast proteome. *Proc Natl Acad Sci U S A*, **103**, 13004-13009.
- 59 Guidi, S., Stagni, F., Bianchi, P., Ciani, E., Ragazzi, E., Trazzi, S., Grossi, G., Mangano, C., Calza, L. and Bartesaghi, R. (2013) Early pharmacotherapy with fluoxetine rescues dendritic pathology in the Ts65Dn mouse model of down syndrome. *Brain pathology*, **23**, 129-143.
- 60 Jhang, C.L., Huang, T.N., Hsueh, Y.P. and Liao, W. (2017) Mice lacking cyclin-dependent kinase-like 5 manifest autistic and ADHD-like behaviors. *Hum Mol Genet*, **26**, 3922-3934.
- 61 Deacon, R.M. (2006) Digging and marble burying in mice: simple methods for in vivo identification of biological impacts. *Nat Protoc*, **1**, 122-124.
- 62 Bastianini, S., Alvente, S., Berteotti, C., Lo Martire, V., Silvani, A., Swoap, S.J., Valli, A., Zoccoli, G. and Cohen, G. (2017) Accurate discrimination of the wake-sleep states of mice using non-invasive whole-body plethysmography. *Scientific reports*, **7**, 41698.

FIGURE LEGENDS

Figure 1 Transduction efficiency of TATκ-GFP-CDKL5₁ fusion protein

A: Western blot analysis using an anti-CDKL5 antibody confirmed TATκ-GFP-CDKL5₁ protein expression in transfected HEK293T cells (cell extract, lane 1) and TATκ-GFP-CDKL5₁ protein accumulation in the concentrated (20x) culture medium (medium from two independent preparations, lanes 3 and 4), indicating that the TATκ-GFP-CDKL5₁ protein was secreted from HEK293T cells. Cell extracts and concentrated (20x) culture medium of untransfected HEK293T cells are shown in lanes 2 and 5, respectively. **B:** Western blot analysis using an anti-CDKL5 antibody on 4-day (DIV4) differentiated primary hippocampal neuronal cultures from *Cdkl5*^{-/-} mice, treated for 1 h with vehicle (left lane) or purified TATκ-GFP-CDKL5₁ protein (50 ng, right lane) confirmed that TATκ-GFP-CDKL5₁ protein is internalized by target cells. **C:** Confocal microscopy images showing the presence of TATκ-GFP-CDKL5₁ protein in 10-day (DIV10) differentiated primary hippocampal neurons from *Cdkl5*^{-/-} mice treated for 1 h with purified TATκ-GFP-CDKL5₁ protein (50 ng, right lane). Cells were co-stained for CDKL5 (red) and GFP (green) expression and nuclei were counterstained with TO-PRO-3 far red dye. Scale bar = 10 μm. **D:** Series of 4 images (1-4) from confocal microscopy (Z stack size 1 μm) of the same hippocampal neuron as in C. Images confirm that TATκ-GFP-CDKL5₁ protein is internalized by target cells. Scale bar = 10 μm.

Figure 2 Effect of TATκ-GFP-CDKL5₁ fusion protein on neuronal cell lines.

A: Images of Hoechst stained nuclei of SH-SY5Y cells treated with purified TATκ-GFP or TATκ-GFP-CDKL5₁ for 24 h. Examples of mitotic nuclei are indicated by an arrow. Scale bar = 35 μm. **B:** SH-SY5Y cells were treated with 50 ng purified TATκ-GFP (1), TATκ-GFP-CDKL5₁ (2) or TATκ-GFP-CDKL5(K42R)₁ (3) proteins for 24 h. Quantification of the mitotic index evaluated as the ratio between the number of cells in mitosis and the total cell number, and expressed as the percentage of TATκ-GFP treated cells. Note the large reduction in the number of proliferating cells. Values in B represent the percentage of mean ± SE. *** p < 0.001 as compared to TATκ-GFP treated cells (Fisher's LSD test after ANOVA). **C:** Western blot analysis using an anti-GFP antibody of the purified TATκ-GFP (lane 1), TATκ-GFP-CDKL5₁ (lane 2) and TATκ-GFP-CDKL5 (K42R)₁ (lane 3) proteins used in experiment B. **D:** Ten-day (DIV10)

differentiated primary hippocampal neuronal cultures from *Cdkl5*^{-/-} mice were treated for 1 h with purified TATκ-GFP-CDKL5₁ or TATκ-GFP protein (50 ng), and protein localization was assessed by immunostaining with an anti-GFP antibody (red) and an anti-β III tubulin antibody (TUBJ, green). Nuclei were counterstained with Hoechst. Higher magnification shows the enlargement of a dendrite segment included in the dotted box. Scale bar = 25 μm (lower magnification) = 5 μm (higher magnification). **E:** Confocal microscopy images of a dendrite segment of a hippocampal neuron treated with TATκ-GFP-CDKL5₁ as in D. Images show co-localization of TATκ-GFP-CDKL5₁ protein with a pre-synaptic protein (synaptophysin, SYN; left panels) and a post-synaptic protein (PSD-95; right panels). TATκ-GFP-CDKL5₁ immunodetection was conducted using an anti-GFP antibody. Scale bar = 5 μm. **F-H:** Hippocampal neuronal cultures from *Cdkl5*^{-/-} mice were treated, starting from the second day in culture, every two days for 8 days, with TATκ-GFP-CDKL5₁ or TATκ-GFP-CDKL5(K42R)₁ proteins (50 ng) and the effects on neurite outgrowth, synaptic innervations, and spine density were assessed. The histogram in F shows the quantification of neurite outgrowth of microtubule-associated protein 2 (MAP2)-positive untreated *Cdkl5*^{+/+} and *Cdkl5*^{-/-} hippocampal neurons and *Cdkl5*^{-/-} hippocampal neurons treated with TATκ-GFP-CDKL5₁ or TATκ-GFP-CDKL5(K42R)₁. The histograms in G and H show the number of SYN immunoreactive puncta per μm in proximal dendrites and the number of MAP2-positive spines per 10 μm in hippocampal neurons as in F. **I:** Representative fluorescence images of differentiated hippocampal cultures as in F, that were immunopositive for MAP2 (green) and synaptophysin (SYN; red). The dotted boxes indicate proximal dendrite segments shown at a higher magnification. Scale bar = 50 μm (lower magnification) = 5 μm (higher magnification). Values in (F-H) are represented as means ± SE. * p < 0.05, ** p < 0.01, *** p < 0.001 as compared to the untreated *+/+* condition; # p < 0.01 as compared to the untreated *-/-* samples (Fisher's LSD test after ANOVA).

Figure 3 Effect of TATκ-CDKL5 protein therapy on behavior.

A: Schedule of intracerebroventricular implantation and fusion protein injection (see methods). Male *Cdkl5*^{-/-} mice received treatment with TATκ-GFP or TATκ-GFP-CDKL5₁ (10 μl injection, approximately 60 ng/injection). **B:** Spatial learning assessed with the Morris Water Maze in untreated *Cdkl5*^{+/+} (n=6) and *Cdkl5*^{-/-} (n=6) mice and *Cdkl5*^{-/-} mice treated with TATκ-GFP (n=5) or TATκ-

GFP-CDKL5₁ (n=7). **C:** Probe test on day 6 in untreated and treated *Cdkl5* -/Y mice as in B. **D:** Passive avoidance test on untreated *Cdkl5* +/Y (n=8) and *Cdkl5* -/Y (n=7) mice, and on *Cdkl5* -/Y mice treated with TATκ-GFP (n=5) or TATκ-GFP-CDKL5₁ (n=5). Graphs show the latency to enter the dark compartment on the 1st day (left panel) and on the 2nd day (right panel) of the behavioral procedure. **E:** Raw tracings of the whole-body plethysmography signal during non-rapid-eye-movement sleep of a *Cdkl5* -/Y mouse treated with TATκ-GFP or TATκ-GFP-CDKL5₁. A red arrow indicates a sleep apnea, while a black arrow indicates an augmented breath (sigh). **F:** Sleep apnea occurrence rate in untreated *Cdkl5* +/Y (n=10) and *Cdkl5* -/Y (n=10) mice (28), and *Cdkl5* -/Y mice treated with TATκ-GFP (n=5) or TATκ-GFP-CDKL5₁ (n=5). Values represent mean ± SE (Student's t-test). **G:** Representative images of clasping behavior. Total amount of time spent hind-limb clasping during a 2 min interval (graph on the right) in untreated *Cdkl5* +/Y (n=8) and *Cdkl5* -/Y (n=8) mice, and in *Cdkl5* -/Y mice treated with TATκ-GFP (n=5) or TATκ-GFP-CDKL5₁ (n=7). Values in (B-D,G) represent mean ± SE * p < 0.05, ** p < 0.01, *** p < 0.001 as compared to the untreated *Cdkl5* +/Y condition; # p < 0.01, ## p < 0.001 as compared to the untreated *Cdkl5* -/Y condition (Fisher's LSD test after ANOVA).

Figure 4 Effect of TATκ-CDKL5 protein therapy on dendritic morphology

A: Examples of sections processed for DCX immunostaining from the dentate gyrus (DG) of untreated *Cdkl5* +/Y and *Cdkl5* -/Y mice, and of *Cdkl5* -/Y mice treated with TATκ-GFP or TATκ-GFP-CDKL5₁, according to the injection schedule in Fig. 3A, and sacrificed 10 days after the end of protein administration. Scale bar = 40 μm. **B:** Mean total dendritic length of newborn granule cells of untreated *Cdkl5* +/Y (n=5) and *Cdkl5* -/Y (n=5) mice, and of *Cdkl5* -/Y mice treated with TATκ-GFP (n = 6) or TATκ-GFP-CDKL5₁ (n=6). **C:** Example of a Golgi-stained hippocampal slice. Abbreviations: GL = granule cell layer, H = Hilus, Mol =Molecular layer. Scale bar: 250 μm. **D:** Examples of the dendritic tree of Golgi-stained granule cells of 1 animal from each experimental group. Scale bar = 100 μm. **E-G:** Mean total dendritic length (E), mean branch length (F) and mean number of dendritic segments (G) of untreated *Cdkl5* +/Y (n=5) and *Cdkl5* -/Y (n=5) mice, and of *Cdkl5* -/Y mice treated with TATκ-GFP (n=5) or TATκ-GFP-CDKL5₁ (n=4). **H:** Example of the reconstructed dendritic tree of a Golgi-stained CA1 pyramidal neuron with apical and basal dendrites. **I:** Mean total dendritic length of basal (left panel)

and apical (right panel) dendrites of CA1 pyramidal neurons in untreated and treated mice as in (E). Values in (B, E-G and I) are represented as means \pm SE. * $p < 0.05$; ** $p < 0.01$; *** $p < 0.001$ as compared to the untreated *Cdkl5* +/Y condition; # $p < 0.05$ as compared to the untreated *Cdkl5* -/Y samples (Fisher's LSD test after ANOVA).

Figure 5 Effect of TAT κ -CDKL5 protein therapy on neuronal connectivity.

A: Images of Golgi-stained dendritic branches of granule cells of CA1 pyramidal neurons of a *Cdkl5* +/Y and a *Cdkl5* -/Y mouse, and a *Cdkl5* -/Y mouse treated with TAT κ -GFP or TAT κ -GFP-CDKL5₁, according to the injection schedule in Fig. 3A. Scale bar = 4 μ m. **B:** Images of dendrite segments at a higher magnification of CA1 pyramidal neurons of a *Cdkl5* +/Y and a *Cdkl5* -/Y mouse. The red asterisks indicate immature spines (filopodium-like, thin, and stubby-shaped; top right diagram) and the blue asterisks indicate more mature spines (mushroom- and cup-shaped). **C,D:** Dendritic spine density (number of spines per 10 μ m) and percentage of immature and mature spines in relation to the total number of protrusions of granule neurons (C) and CA1 pyramidal neurons (D) from untreated *Cdkl5* +/Y (n=5) and *Cdkl5* -/Y (n=5) mice, and from *Cdkl5* -/Y mice treated with TAT κ -GFP (n=5) or TAT κ -GFP-CDKL5₁ (n=5). **E:** Representative fluorescence image of a hippocampal section processed for PSD-95 immunoreactivity. Abbreviations: GL = granule cell layer, Mol =Molecular layer. Scale bar: 250 μ m. The dotted box in the upper panel indicates the analyzed region (molecular layer of the dentate gyrus (DG)). Magnifications in lower panels show examples of PSD-95 immunoreactive puncta in the Mol of a *Cdkl5* +/Y and a *Cdkl5* -/Y mouse, and of a *Cdkl5* -/Y mouse treated with TAT κ -GFP-CDKL5₁. Scale bar = 5 μ m. **F:** Number of fluorescent puncta per μ m² exhibiting PSD-95 immunoreactivity in the Mol of untreated *Cdkl5* +/Y (n=6) and *Cdkl5* -/Y (n=7) mice, and of *Cdkl5* -/Y mice treated with TAT κ -GFP (n=3) or TAT κ -GFP-CDKL5₁ (n=5). Values in (C, D and F) are represented as means \pm SE. * $p < 0.05$; ** $p < 0.01$; *** $p < 0.001$ as compared to the untreated *Cdkl5* +/Y condition; # $p < 0.05$ as compared to the untreated *Cdkl5* -/Y samples (Fisher's LSD test after ANOVA).

Figure 6 TAT κ -CDKL5 systemic delivery into the CNS

A: Mice (postnatal day 7, P7) were systemically treated (one single sub-cutaneous injection) with vehicle,

TATκ-GFP, and TATκ-GFP-CDKL5₁, and brain samples were collected 4 h post injection. **B:** Images show TATκ-GFP or TATκ-GFP-CDKL5₁ protein localization in the sensory-motor cortex (CX) of treated mice 4 h post injection. Localization of TATκ-GFP and TATκ-GFP-CDKL5₁ was evaluated through immunohistochemistry using an anti-GFP antibody (red), and nuclei were counterstained with Hoechst. Scale bar = 30 μm. **C:** Adult mice (postnatal day 90, P90) were systemically treated (intravenous injection) with vehicle, TATκ-GFP, and TATκ-GFP-CDKL5₁, and brain samples were collected 1 h post injection. **D:** Images show TATκ-GFP or TATκ-GFP-CDKL5₁ protein localization in the striatum of treated mice 1 h post injection. Localization of TATκ-GFP and TATκ-GFP-CDKL5₁ was evaluated through immunohistochemistry using an anti-GFP antibody (red), and nuclei were counterstained with Hoechst. Scale bar = 60 μm.

Figure 7 Effect of systemically-administered TATκ-CDKL5 on hippocampus development

A: Treatment schedule for systemic administration of the CDKL5 fusion proteins. Protein was injected using a programmable pump twice a day (morning and evening; 20μl injection, approximately 50ng/injection) for the duration of 10 days through a cannula directly into the internal carotid artery. **B:** Examples of sections processed for DCX immunostaining from the DG of a *Cdkl5* -/Y mouse treated with TATκ-GFP or TATκ-GFP-CDKL5₁, according to the injection schedule in A. Scale bar = 40 μm. **C:** Mean total dendritic length of newborn granule cells of untreated *Cdkl5* +/Y (n=5) and *Cdkl5* -/Y (n=5) mice, and of *Cdkl5* -/Y mice treated with TATκ-GFP (n=6) or TATκ-GFP-CDKL5₁ (n=6). **D:** Mean total dendritic length of Golgi-stained granule cells of untreated *Cdkl5* +/Y (n=5) and *Cdkl5* -/Y (n=5) mice, and of *Cdkl5* -/Y mice treated with TATκ-GFP (n=5) or TATκ-GFP-CDKL5₁ (n=5). **E:** Dendritic spine density of granule neurons from untreated *Cdkl5* +/Y (n=5) and *Cdkl5* -/Y (n=5) mice, and from *Cdkl5* -/Y mice treated with TATκ-GFP (n=5) or TATκ-GFP-CDKL5₁ (n=5). **F:** Spatial learning and memory assessed with the Barnes Maze in untreated *Cdkl5* +/Y (n=15) and *Cdkl5* -/Y (n=8) mice, and in *Cdkl5* -/Y mice treated with TATκ-GFP (n=7) or TATκ-GFP-CDKL5₁ (n=5). Graphs show the mean latency to find the target hole during the 3-day learning period (left histogram) and the latency to find the target hole on the probe day (right histogram). **G:** Number of digging bouts of untreated *Cdkl5* +/Y (n=11) and *Cdkl5* -/Y (n=11) mice, and of *Cdkl5* -/Y mice treated with TATκ-GFP (n=6) or TATκ-GFP-CDKL5₁ (n=5). **H:**

Nest quality of untreated *Cdkl5* +/Y (n=6) and *Cdkl5* -/Y (n=11) mice, and of *Cdkl5* -/Y mice treated with TATκ-GFP (n=6) or TATκ-GFP-CDKL5₁ (n=5). **I:** Average locomotion velocity (left graph) and total distance traveled (right graph) of untreated *Cdkl5* +/Y (n=6) and *Cdkl5* -/Y (n=6) mice, and of *Cdkl5* -/Y mice treated with TATκ-GFP (n=8) or TATκ-GFP-CDKL5₁ (n=11), during a 20-min open field test. **J:** Number of stereotypical jumps (repetitive beam breaks < 1 s) in the open field arena of untreated *Cdkl5* +/Y (n=6) and *Cdkl5* -/Y (n=6) mice, and of *Cdkl5* -/Y mice treated with TATκ-GFP (n=7) or TATκ-GFP-CDKL5₁ (n=10). Values in (C-J) are represented as means ± SE. * p < 0.05; ** p < 0.01; *** p < 0.001 as compared to the untreated *Cdkl5* +/Y condition; # p < 0.05 as compared to the untreated *Cdkl5* -/Y samples (Datasets in C-I, Fisher's LSD test after ANOVA; datasets in J, Dunn's test after Kruskal-Wallis test).

Figure 8 Effect of systemically-administered TATκ-CDKL5 on visual cortex

A: Treatment schedule for systemic administration of fusion proteins. TATκ-GFP or TATκ-GFP-CDKL5₁ proteins were injected using a programmable pump twice a day (morning and evening; 20μl injection, approximately 50ng/injection) for the duration of 10 days through a cannula directly into the internal carotid artery. Visual imaging (IM) was assessed in *Cdkl5* -/Y mice two days before the beginning of treatment (baseline). Whole body plethysmography (WBP) and IM were assessed on the tenth day of protein infusion and after 5 and 10 days after the end of protein administration. **B:** REM sleep apnea occurrence rate in untreated *Cdkl5* +/Y (n=10) and *Cdkl5* -/Y (n=10) mice (28), and in *Cdkl5* -/Y mice treated with TATκ-GFP (n=6) and TATκ-GFP-CDKL5₁ (n=5). The patterned area represents the time window in which the treatment was administered. Values are represented as means ± SE, *p<0.05, **p<0.01 (Holm-Sidak's multiple comparisons test after two-way ANOVA). **C:** Upper panel: diagram of the field of view for Intrinsic Optical Signal (IOS) Imaging experiments. Darker areas in the figure represent the active parts of the primary visual cortex (V1) following visual stimulation corresponding to the binocular visual cortex. Lower panel: representative IOS response images collected at different time points in two *Cdkl5* -/Y mice treated with TATκ-GFP and TATκ-GFP-CDKL5₁, respectively. Scale bar: 1mm. **D:** Mean amplitude of visually-evoked IOS responses measured before and after 10 days of treatment in *Cdkl5* -/Y mice treated with TATκ-GFP (n=8) and TATκ-GFP-CDKL5₁ (n=9). The

persistence of the effect was evaluated with additional measurements 5 and 10 days after treatment cessation (washout). Values are represented as means \pm SE Two-way ANOVA (repeated measures for the factor time) revealed a time X treatment interaction $p < 0.05$; post-hoc Holm-Sidak's multiple comparisons test: * $p < 0.05$, ** $p < 0.01$. **E:** Dendritic spine density (number of spines per 10 μ m) of V1 pyramidal neurons (layer II/III) from untreated *Cdkl5* +/Y (n=5) and *Cdkl5* -/Y (n=5) mice, and from *Cdkl5* -/Y mice treated with TAT κ -GFP (n=4) or TAT κ -GFP-CDKL5₁ (n=5) and sacrificed at the end of treatment (short term), or with TAT κ -GFP (n=5) or TAT κ -GFP-CDKL5₁ (n=5) and sacrificed 10 days after treatment cessation (long term). **F:** Number of fluorescent puncta per μ m² exhibiting PSD-95 immunoreactivity in V1 (layer II/III) of untreated *Cdkl5* +/Y (n=5) and *Cdkl5* -/Y (n=5) mice and *Cdkl5* -/Y mice treated with TAT κ -GFP (n=4) or TAT κ -GFP-CDKL5₁ (n=6) and sacrificed at the end of treatment (short term) or with TAT κ -GFP (n=4) or TAT κ -GFP-CDKL5₁ (n=4) and sacrificed 10 days after treatment cessation (long term). Values in (E,F) are represented as means \pm SE. ** $p < 0.01$; *** $p < 0.001$ as compared to the untreated *Cdkl5* +/Y condition; # $p < 0.05$ as compared to the untreated *Cdkl5* -/Y samples (Fisher's LSD test after ANOVA). Abbreviation: IM: visual imaging; WBP: whole body plethysmography.

ABBREVIATIONS:

AIF-1 = Allograft Inflammatory Factor 1, BM = Barnes Maze; CX = sensory-motor cortex, DCX = doublecortin, DG = dentate gyrus, DMEM = Dulbecco's modified Eagle's medium, GFAP = Glial fibrillary acidic protein; GFP = green fluorescent protein, GL = granule cell layer, H = hilus, HRP = horseradish peroxidase, ICV = intracerebroventricular, KO = knockout, MAP2 = microtubule-associated protein 2, MOL = molecular layer, MWM = Morris Water Maze, NeuN = Neuronal nuclear protein; NREMS = non-rapid-eye-movement sleep, P = postnatal day, PA = Passive Avoidance, PSD-95 = postsynaptic density protein 95, PTDs = protein transduction domains, REMS = rapid-eye-movement, R reflectance, RTT = Rett syndrome, ROI = region of interest, ROR = region of reference, SE = standard error, SYN = synaptophysin, TAT = HIV-1 Transactivator of Transcription protein, TTOT = instantaneous total breath duration, WBP = whole-body plethysmography.

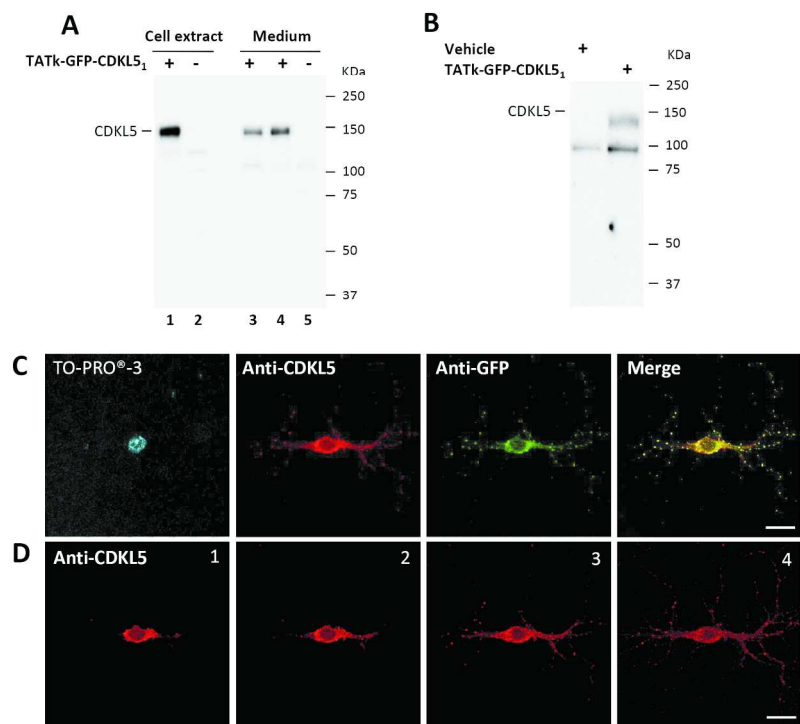


Figure 1

190x254mm (300 x 300 DPI)

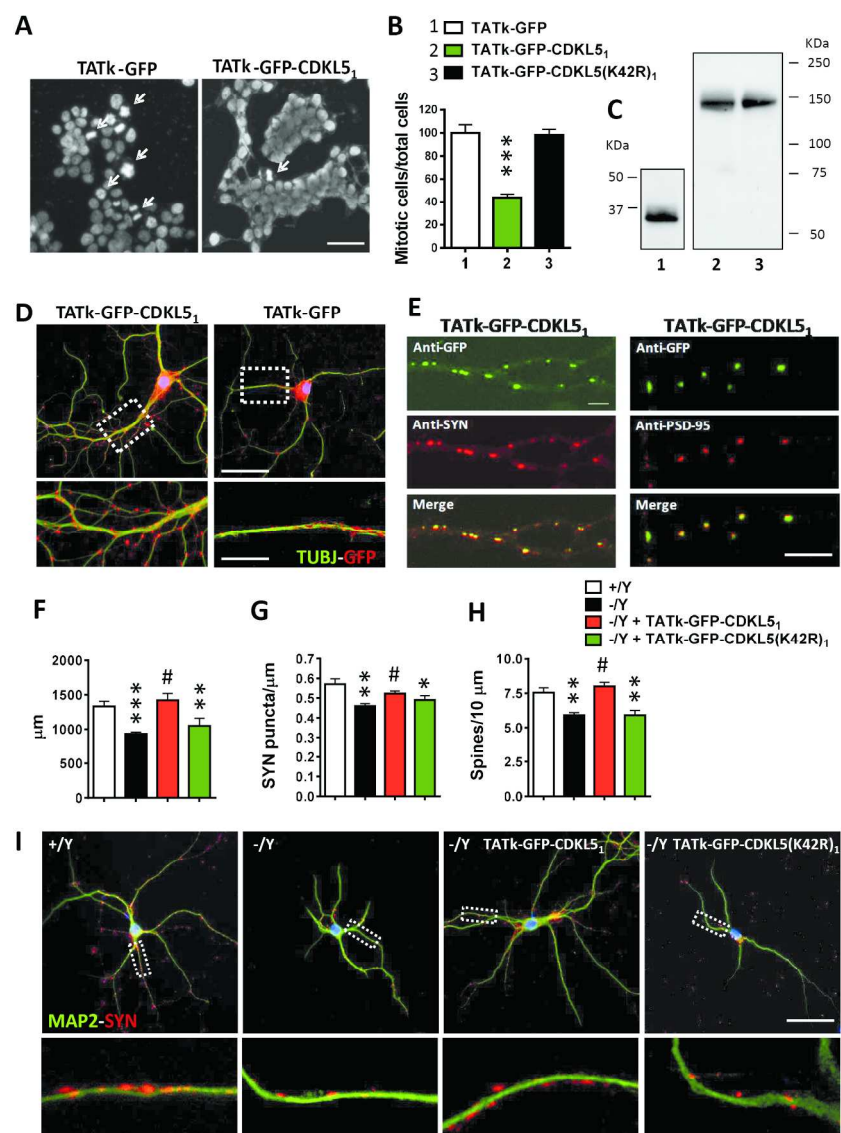


Figure 2

190x254mm (300 x 300 DPI)

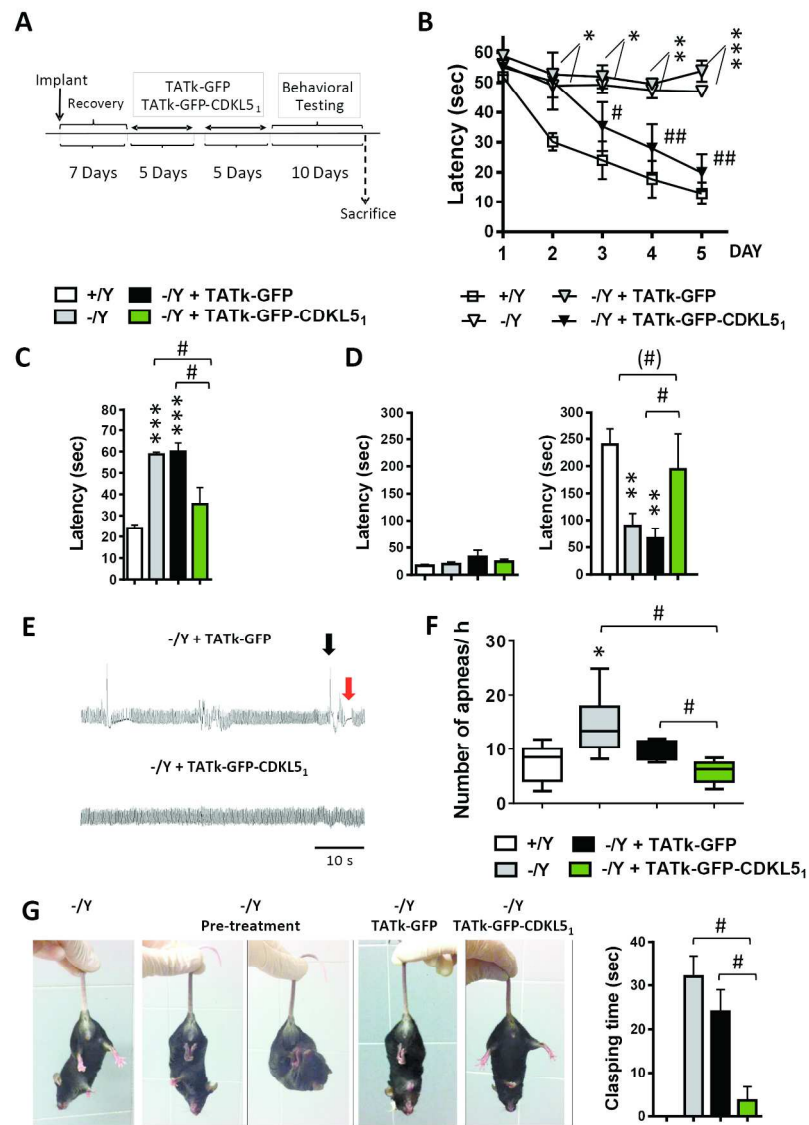


Figure 3

190x254mm (300 x 300 DPI)

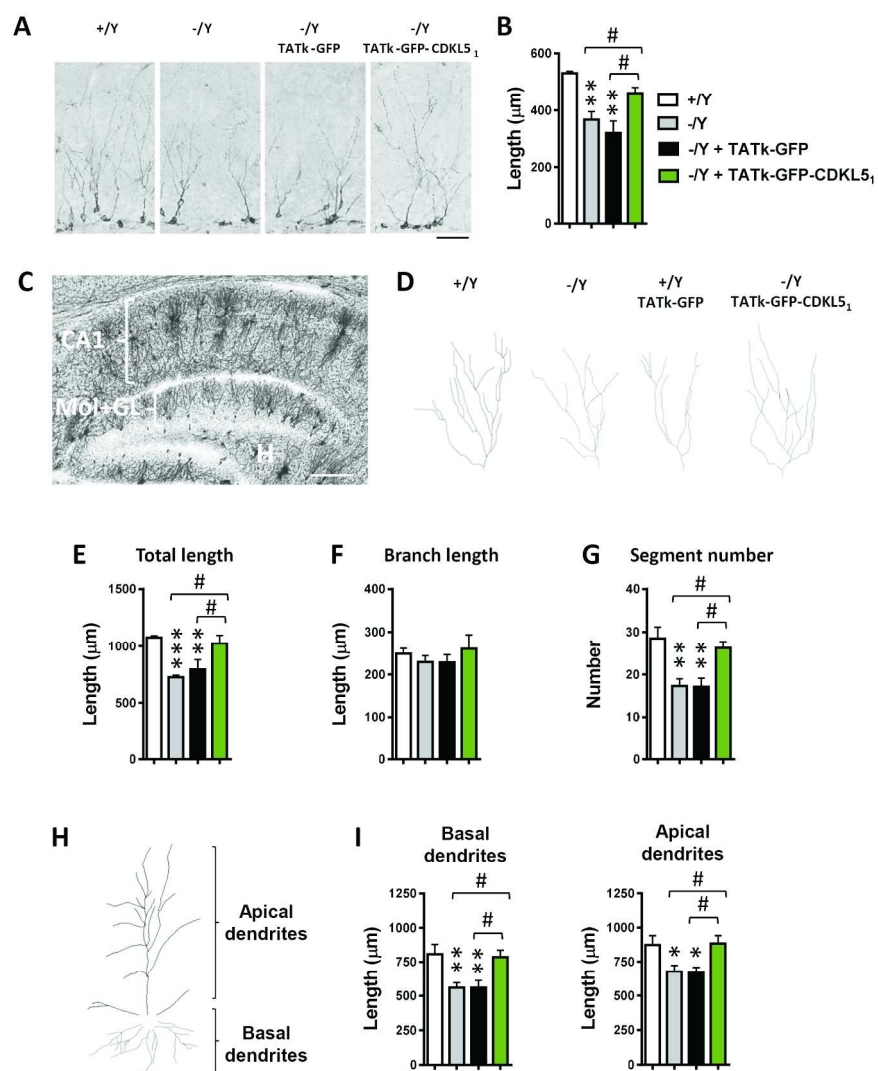


Figure 4

190x254mm (300 x 300 DPI)

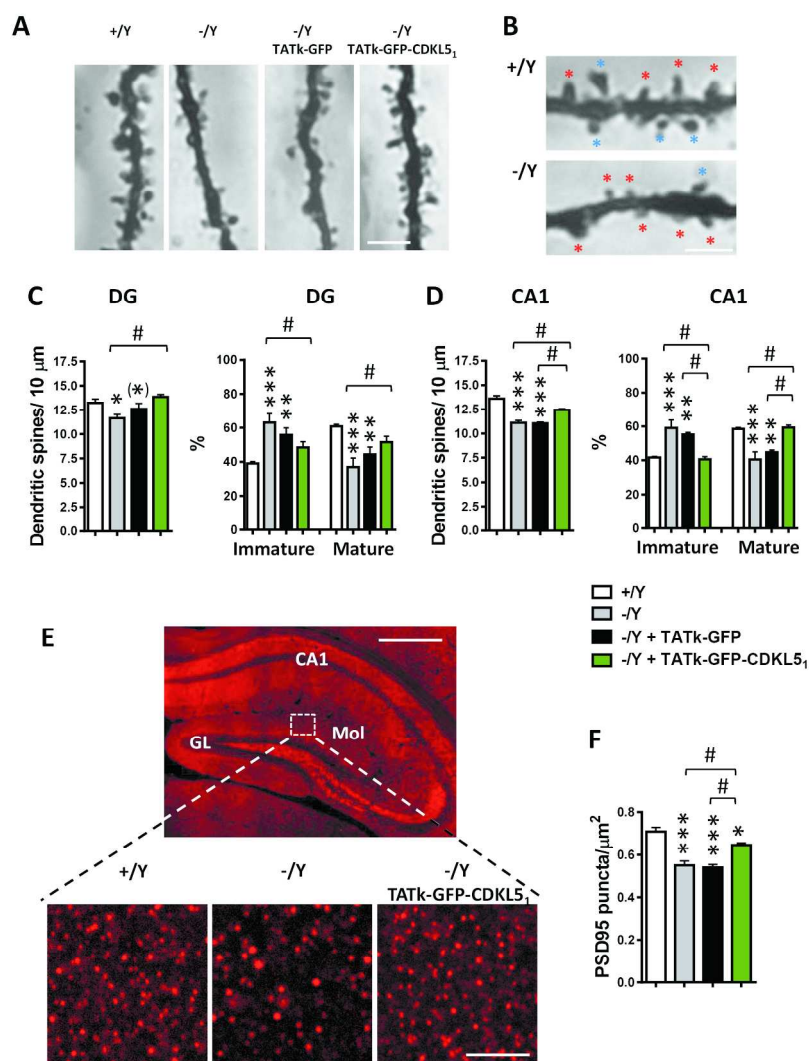


Figure 5

190x254mm (300 x 300 DPI)

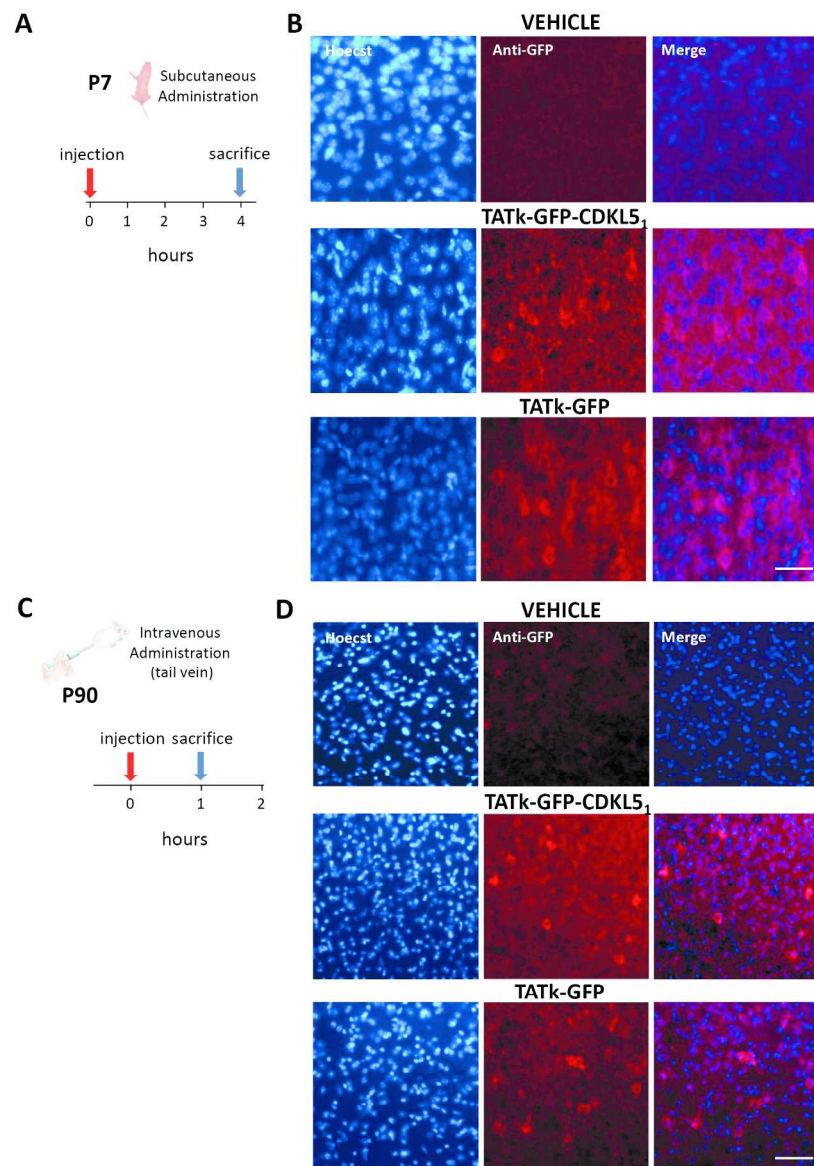


Figure 6

190x254mm (300 x 300 DPI)

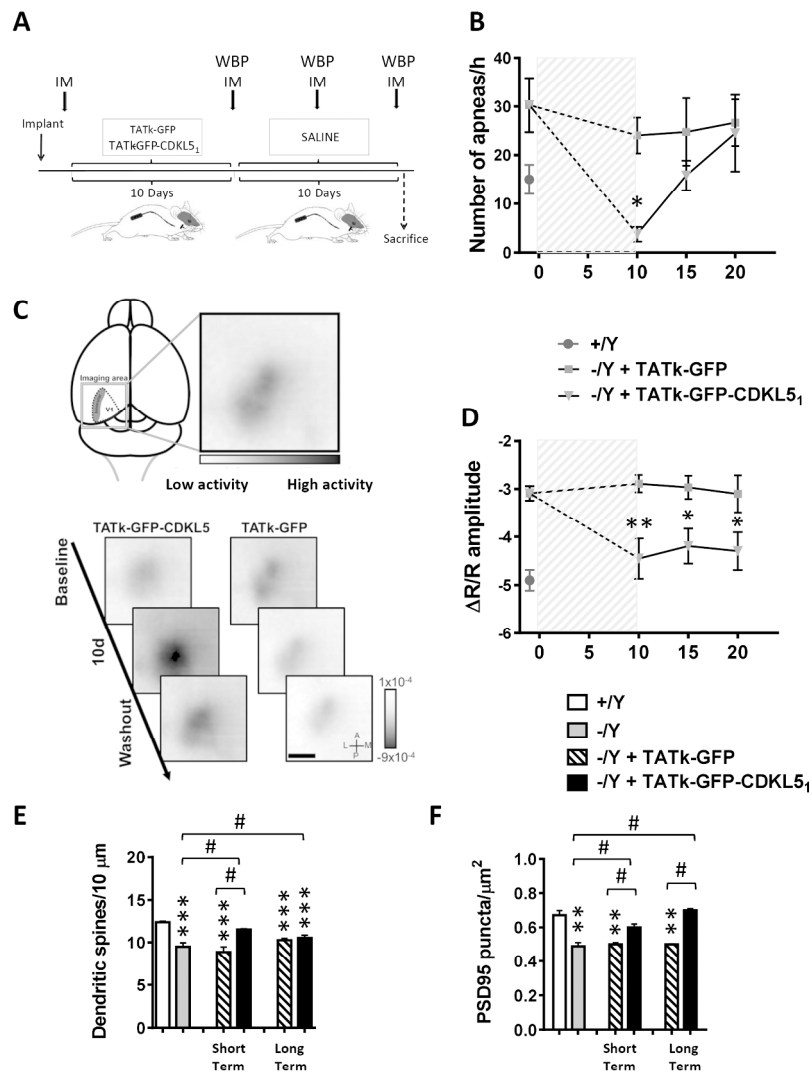


Figure 8

190x254mm (300 x 300 DPI)